

## 6. Problem №8: Electrostatics

### *Solution of Croatia*

#### **Problem №8: Electrostatics**

Josko Jelacic<sup>1</sup>, Marin Lukas<sup>1</sup>, Milan Marković<sup>2</sup>, Damjan Pelc<sup>1</sup>, Ivan Sudic<sup>1</sup>

<sup>1</sup> V. Gimnazija, Klaićeva 1, 10000 Zagreb, Croatia

<sup>2</sup> XV. Gimnazija, Jordanovac 8, 10000 Zagreb, Croatia

#### **The Problem:**

*Propose and make a device for measuring the charge density on a plastic ruler after it has been rubbed with a cloth.*

#### **Abstract**

We present a computer numerically controlled surface charge density analyzer for measuring mono-layer surface charges in medium resolution on dielectric surfaces. The device is based on a solid state FET electrometer coupled with an optically referenced electrostatic mill enabling accurate phase-locked measurements. The scanning and control are obtained with a two-dimensional computer controlled discrete step translator capable of delivering up to 20 steps per second. The device was demonstrated in a measurement of the surface charge density on a plastic ruler rubbed with a cotton cloth.

#### **1. Introduction.**

The problem of non - contact charge measurement on different dielectrics is of greatest interest nowadays. From microscopic applications to atmospheric electricity recording, charge detectors of various designs are implemented. In this article we will discuss the construction of such a device, intended for measurements in the medium resolution range (that is, neither atomic – scale nor large charge structures like atmospheric electricity), intended for measuring the charge density of a flat charge monolayer on a dielectric surface. We will demonstrate its action in a measurement of the charge accumulated on a plastic ruler rubbed with a cloth, a system being very favorable for testing the device resolution and precision due to large charge gradients on a small surface area. But before we proceed to the description of the device, we must note some general characteristics our charge detector should have; in the end we will see how many requirements we have fulfilled. First of all, the spatial resolution for the suggested application should be at least a few millimeters due to the large gradients, and better if possible. The charge measurement resolution isn't as critical; the charges normally accumulating on a ruler can be quite large, as we shall see. Anyway, a higher charge resolution means a more reliable device. The third important parameter is the time the measurement takes. We will find that charge continuously drifts away from our ruler; this is unavoidable except by putting the entire device in an inert atmosphere or vacuum, which was too complicated for us to do. Although the drifting can be minimized by several techniques (to be discussed), a fast measurement is necessary. As our device will in fact be a scanner, moving across the ruler surface and measuring local charge density, we must be careful to minimize the number of needed scanning steps to shorten the measurement time, while

retaining an acceptable spatial resolution. We will discuss these matters in more detail when we get to the actual device construction.

## 2. The Ruler.

As we have mentioned, our charge analyzer will be used on a charged plastic ruler. Our ruler was made of polymethylmetacrilate and was 15 cm long and 3 centimeters wide. The charging of a ruler by rubbing it with a cloth is a high school demonstration in electrostatics, and there is a number of charge *detection* (not measurement!) methods suiting it. The most common are different electrometers based on charge – metal needle repulsion, and charged powders (like sulphur) clinging to the charged regions of the ruler. However, really *measuring* the charge density distribution with a reasonable spatial resolution is a considerable difficulty. Even more complicated is the process of charging; why are electrons transferred between cloth and ruler surface, and what sign will the net charge on the ruler have? The answer to these questions has to do with intermolecular forces on surfaces, delocalized electrons in the fabric and on the plastic, dielectric polarization and so forth, and we will not go into tackling with it. Even the sign of the charges is not uniquely determined; we have measured both positive and negative charges on one and the same ruler, which was quite a surprise. The important fact is that once the charges are deposited on the ruler surface they basically *do not* move. This is due to the fact that the ruler is a dielectric, meaning that it has a huge electrical resistance and no current can flow either inside it or on its surface. Another important consequence of this is that the charges will always stay on the surface and never penetrate the material; thus we can rightly speak of a monolayer. However, in practice the conductivity of the ruler surface usually isn't nearly as small as one would expect, mainly because of the grease and dirt deposited on the ruler when it is handled. This can cause significant charge drift and make measurements rather inexact. To minimize this effect the ruler needs to be degreased thoroughly (we rinsed it in ethyl alcohol several times before every measurement) and put on nonconducting stands (in our case degreased ceramic cylinders). In this way the charge drift can be slowed down considerably, though it can never be completely removed – there is namely a second source of drift, humidity in the atmosphere. Due to the polar nature of the water molecules in air the charges on the surface may cling to them and escape the ruler. This drift is very difficult to remove; in all of our experiments the air was constantly held dry (humidity under 20%), but a certain drift was always present. However, the charge didn't change as rapidly as to influence the measured results significantly, as we managed to get the scanning time down to a few minutes.

The rubbing process itself was devoted special care. With a clean cotton cloth the ruler was rubbed exquisitely at one or two localized spots, the rest remaining more or less untouched. In this way we created regions of large charge density and steep transitions to low – charge regions; this enabled us to test the capabilities of our detector. A good device should be capable of reconstructing such configurations in detail.

## 3. The Device.

### 3.1. Principle of measurement.

The number of charge measurement principles and devices developed to date is enormous, and each has its advantages and drawbacks. Some of the most common are the Kelvin and vibrating capacitor probes [1] (for medium spatial resolution), cantilever – based systems [2] (used in atomic force microscopes, measure the force on a charged tip with atomic – scale spatial resolution), the already mentioned crude electrometers used in demonstrations, solid

state electrometers [3] of various designs, and many more. Our device used a combination of a so-called *electrostatic mill* and a solid state electrometer. The electrostatic mill is a movable grounded plate, periodically covering and uncovering the electrometer's detector lead. In this way the electrometer is only exposed to the field it measures for short periods of time, yielding an alternating signal. If the phase relationship between the mill oscillations and the periodic electrometer signal is established, one can perform phase – locked measurements to eliminate virtually all noise. Thus the field can be measured to a very high precision. However, there is another vital element in the construction of our device, namely the scanning system. The mill, electrometer test lead and phase reference measuring system were all mounted on a compact probe, which had to be moved across the ruler surface in order to scan the charge density distribution. This was done with a custom made xy-translator, controlled electronically. In the following sections we will describe these parts one by one, in order to gain insight in the construction and operation of our apparatus.

### 3.2. The Probe.

The probe, being the core of the system, requires special attention. As we have mentioned, its main parts are the electrostatic mill, electrometer test lead and phase reference measuring system. All those elements were mounted on a large grounded metal plate which provided shielding and a homogeneous field in the perpendicular direction (Fig. 1.). The mill, as the only moving part, required precision; it consisted of a conducting thin disc (made of paper covered with a conducting graphite film) with three holes cut in it, attached to a small DC motor (similar to the ones used in mobile phones for vibration). The mill (or "chopper", as we refer to it) is shown in Fig. 2. It rotated with a frequency of about 80 Hz, providing a convenient modulation of the electrometer signal. The electrometer itself was based on a FET (short for field effect transistor), which is a semiconductor device consisting of a long slab of n – doped material (through which a current is set to flow) and two smaller sheets of p – doped material located on opposite sides of the n – slab. If leads are connected to those sheets and put in an electric field, charges in the sheets are dislocated, effectively altering the volume (and thus the resistance) of the n – doped slab (Fig. 3.). This means that one can determine the strength of the field by measuring the current flowing through the n – slab! It is clear that the resistance between the points A and B in figure 3 is enormous (ideally infinite), meaning that charges aren't lost from the test leads but respond only to the outside field. However, the problems arising to instabilities and noise when using a sole FE transistor made us choose the FET amplifier LMC 6062 instead. The principle of operation remains practically the same. The amplifier was connected to be noninverting, with a gain equal to unity and with a low – pass RC filter at the input to serve as a first, crude noise removal facility. The entire circuit was closed in a grounded metal box shielding it from outside influences (Fig. 4.), while the test lead consisted of a copper disc 1 mm in diameter, mounted in a fitting hole in the probe grounded plate. The third vital part of the probe was the phase reference. It had to feed an appreciable signal to the used lock – in amplifier in order for it to be capable of comparing phases. We used a simple photodiode (the bright spot in Fig. 2.); the signal from it was smaller when it was covered by the dark chopper and larger when a hole was under it. The frequency of the signal was of course equal to the chopper frequency. However, the signal offset (due to the constant light always falling on the diode) had to be removed, and the alternating signal amplified. This was done with a LM741 opamp with adjustable gain, followed by a passive high – pass filter for removing the offset. The amplifier and its circuit were enclosed in a grounded box as well.

Once having the two signals, measurement and reference, we fed them into a lock – in amplifier in order to remove noise. As the phase relationship between the measurement signal and the reference was always constant, a phase – locked loop could do a good job removing all out-of-phase or wrong frequency noise, and the resulting signal was very clean and stable. With such noise removal we were capable of measuring the voltage from the FET amplifier with nanovolt precision. As we will see, this amounts to a charge measurement sensitivity of about 10 or even 1 nC/m<sup>2</sup>, while the typical charge densities on the ruler are of the order of 10 μC/m<sup>2</sup>.

### 3.3. Scanning and Control.

Having constructed the probe, we were left with the task of building a device which would move it across the ruler surface in order to obtain a charge density map. The general requirements for such a system we have mentioned already: high spatial resolution and speed. Another problem is the synchronization with the measuring system; this we solved by putting one single computer in charge of both. The translator itself was built from the remains of two used printers (one printer for the  $x$  and one for the  $y$  direction) and driven by two unipolar stepping motors. Driving the motors in accordance with directions given by the main computer was entitled to a microcontroller mainboard. The mainboard was a complicated circuit containing two 8051 microcontrollers clocked at 12 MHz, communicating with the computer via a serial link. Communication proceeded both ways, enabling precise scanning control: the computer collects a number of signal voltage values from the lock-in (using a 12 bit AD converter) and forms their average (that is another low – pass filter!), and then orders the mainboard to move the probe to the next measuring position. When the mainboard reports that the probe has moved a new set of voltages is collected, and so on. The schematic of the entire apparatus is given on Fig. 5, and a photograph on Fig. 6. The spatial resolution was set to 1 mm, and the device was capable of delivering up to 20 measurements per second. However, to use it we had to perform calibration.

### 3.4. Calibration.

To be able to measure the charge in absolute units (like C/m<sup>2</sup>) we had to calibrate our device in a known field. This was done as follows. An aluminum disc, having a surface much larger than the test lead, was held at a constant, known potential  $V$ . The probe was put above it, at a height  $D$ . The probe grounded plate thus created a *charge image* of the disc, the system being equivalent to a capacitor at voltage  $V$  and plates  $D$  centimeters apart. Due to the fact that both the probe plate and the charged disc were much larger than the test lead (or the distance  $D$ , for that matter), the field at the test lead location was almost homogeneous, with a vertical component

$$E_z = \frac{V}{D} \quad (1)$$

Now the root-mean-square voltage measured from the detector,  $U_{RMS}$ , we found to be proportional to  $E$  over a large voltage range (Fig. 7.), following the relationship

$$E_z = 1.88 \cdot 10^6 U_{RMS} \quad (2)$$

We were able to distinguish between positive and negative charges thanks to the phase-locked measurement method; the photodiode always gives the same signal, but the phase of the measurement signal is reversed when measuring different signs of charge. This means that the sign of the measured signal will correspond to the sign of the charge. It is also very important to note that only the  $z$  – component of an electric field can influence the test lead due to the

grounded plate; it creates a mirror image of the charges measured, thus virtually eliminating lateral components. Also, the test lead is a thin disc, so lateral charge displacement in it shouldn't have a significant effect on the FET.

Having performed the calibration, we were ready to make field scans of the ruler and calculate the real charges from the measured field. This was also a troublesome task, due to the fact that the distance between probe and ruler was always kept at 5 mm; this is a large distance compared to the sensing lead disc, which means that a relatively large charged area influences the signal. To maximise the spatial resolution in charge determination we will have to solve a system of equations for the charges; we will return to that issue in due time.

## 4. Measurement and Charge Calculation

Before conducting charge maps measurements, we had to check how fast the charge was leaking off the ruler and how this could influence our scans. Two static measurements were performed, one with the ruler uncleaned and one with a degreased ruler (Fig. 8.). The probe wasn't moving during one measurement. The results are striking: the dirty ruler loses charge at a large pace (70% in five minutes), while upon degreasing it the loss is brought down to about 10% during five minutes! As the scan time was about three minutes, the losses during scanning could be neglected. However, if a necessity for high precision is shown one can always compensate for the loss using the curve on Fig. 8.

Measuring the charges on the ruler was conducted for two rubbings; the first measurement had 5796 and the second 4991 one-millimeter steps. As we mentioned already, the distance between detector and ruler was held at a constant 5 mm. The obtained field maps are shown on Fig. 9. After determining the field maps, we had to calculate the real charge. This charge is easy to find if we divide our ruler into little rectangles, each having a net charge  $\sigma_i$ ; let the sides of the rectangles have lengths equal to the step size, and let their number be equal to the number of steps  $N$ . The field one such rectangle causes at the probe location is simply

$$\mathbf{E}_i(\mathbf{r}_s) = \frac{1}{4\pi\epsilon_0} \frac{\sigma_i \Delta x \Delta y}{|\mathbf{r}_s - \mathbf{r}_i|^2} \hat{\mathbf{r}} \quad (3)$$

where  $\mathbf{r}_s$  is the probe radius-vector,  $\epsilon_0$  is the permittivity of the vacuum,  $\Delta x$  and  $\Delta y$  the side lengths of the rectangle (in our case both equal to the step size),  $\mathbf{r}_i$  the radius-vector of the rectangle and  $\hat{\mathbf{r}}$  a unit vector lying on the line which connects the rectangle and the probe (it can also be written as  $\frac{\mathbf{r}_s - \mathbf{r}_i}{|\mathbf{r}_s - \mathbf{r}_i|}$ ).

Summing the fields of all rectangles and multiplying by two (the charge images forming on the grounded plate double the field!) one gets the net field at the probe location; the detector is only influenced by the vertical component:

$$E_z(x_s, y_s) = \frac{h}{2\pi\epsilon_0} \sum_{i=1}^N \frac{\sigma_i \Delta x \Delta y}{\left[ (x_s - x_i)^2 + (y_s - y_i)^2 + h^2 \right]^{\frac{3}{2}}} \quad (4)$$

where  $x_s$  and  $y_s$  are the probe coordinates,  $h$  its distance from the ruler,  $N$  the number of rectangles (and steps) and  $x_i$  and  $y_i$  the rectangles' coordinates. The probe makes  $N$  steps in its measurement, and on each location measures the field (4). In this way we obtain a system of

$N$  equations for exactly  $N$  unknown charge densities! Of course, the scanning region has to be as large as the ruler so that the  $N$  rectangles cover the entire charged surface. The system of equations is linear, with an extended matrix of the form

$$\begin{pmatrix} \xi_{11} & \xi_{12} & \cdots & \xi_{1N} & E_{z1} \\ \xi_{21} & \xi_{22} & \cdots & \xi_{2N} & E_{z2} \\ \vdots & \vdots & \ddots & \vdots & \vdots \\ \xi_{N1} & \xi_{N2} & \cdots & \xi_{NN} & E_{zN} \end{pmatrix} \quad (5)$$

with the coefficients  $\xi$  equal to

$$\xi_{si} = \frac{h}{2\pi\epsilon_0} \frac{\sigma_i \Delta x \Delta y}{\left[ (x_s - x_i)^2 + (y_s - y_i)^2 + h^2 \right]^{3/2}} \quad (6)$$

As the number  $N$  in our measurements was around 5000 (the system matrix thus containing tens of millions of coefficients), we had to solve the system (5) with the help of a computer. A program diagonalizing the system matrix and solving the resulting triangular form for the unknowns  $\sigma_i$  (Gauss algorithm) was written in Turbo Pascal. The results were charge density maps (Fig. 10.), with spatial resolution 1 mm. As we see, the charge on the ruler was typically of the order of  $10 \mu\text{C}/\text{m}^2$ , as we mentioned before; this is quite a large charge density, corresponding to a metal plate at potentials as high as several thousand volts. The surprising fact is that one can obtain both signs of charge in a single rubbing; the maps clearly show this. We suspect that the reasons for this are very complicated and have to do with intricate surface effects; a possible explanation would be the repelling of charges on the ruler: if a large negative charge is put on the surface it may repel other dislocated electrons. They move away from the negative charge, leaving bare protons behind which form a positive patch. This is however not quite plausible because of the huge resistance to electron flowing; a very high field indeed would be required. A better explanation would probably have to do with the rubbing and transport process itself, but the complications are enormous, so we won't tackle with it. Our task of *measuring* the charge density is complete, with rather satisfactory results.

## 5. Conclusion.

To conclude we will shortly sum up the properties of our device. The charge scanner we constructed was based on a solid state FET electrometer modulated with a chopper; the charge density distribution on a charged ruler (or similar dielectric surface) can be measured fast and reliable. The spatial resolution is 1 mm (this can be made even better, but the scanning time grows proportionally), the sensitivity is about  $10 \text{ nC}/\text{m}^2$  (it can also be enhanced by using more accurate electronics) and a scan of about 5000 points takes three minutes; the measured charge loss during this time is about 5%. We can see that we have more or less fulfilled all the desired characteristics mentioned in the Introduction. In the end let us propose an application we think is quite amusing: charge writing. If one has a relatively large dielectric plate, writing on it with charges is possible with a high voltage tip; if the voltage is high enough a discharge through air will deposit electrons on the plate on a small region near the tip. Putting the tip on

a xy translator enables one to write or make pictures (Fig. 11.). The writing can easily be read with our detector. Of course, a similar process is already implemented in printers and photocopying machines: the xerox process!

We thank our mentors dr. sc. Željko Marohnić from the Institute of Physics for advice, discussions and providing the instruments used in measurement, and prof. Dario Mičić for support and help with everything.

## References.

- [1] A. Winter, J. Kindersberger, Measurement of Double Layer Surface Charge Density Distribution on Insulating Plates with Capacitive Probes, Int. Conference on Advances in Processing, Testing and Application of Dielectric Materials, Wroclaw, 2001., paper 31.
- [2] W. F. Heinz, J. H. Hoh, Relative Surface Charge Density Mapping with the Atomic Force Microscope, Biophys. J. 1999., vol. 76, no. 1.
- [3] W. Mauderli, F. P. Bruno, Solid State Electrometer Amplifier, Phys. Med. Biol., 1966., vol. 11.

## Figures:

Fig. 1. – The probe

Fig. 2. – The chopper.

Fig. 3. – The principle of operation of a FE transistor electrometer

Fig. 4. – The FET amplifier circuit in a grounded box

Fig. 5. – The schematic of the entire apparatus.

Fig. 6. – The entire apparatus

Fig. 7. – The calibration curve.

Fig. 8. – The measurements of charge in time. The detector was static for both curves.

Fig. 9. The field scans. The colour scale is in arbitrary units (volts from the detector)

Fig. 10. – The charge maps.

Fig. 11. – Charge drawing

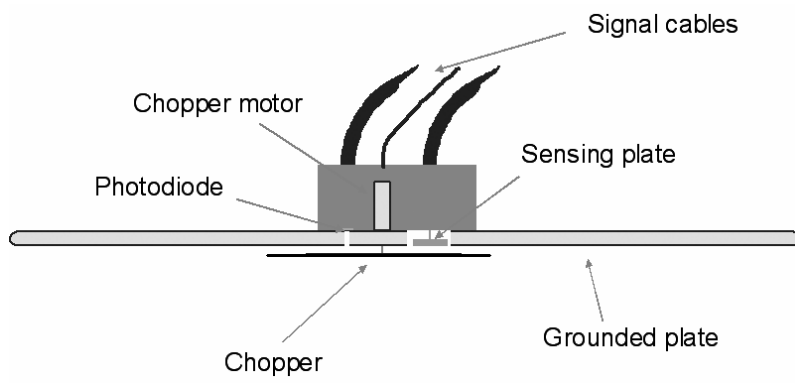


Fig.1

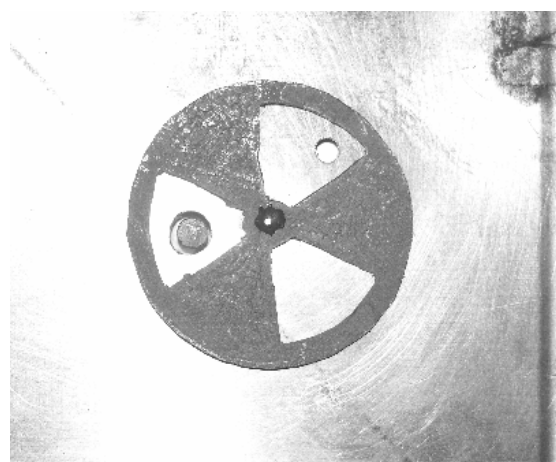


Fig.2

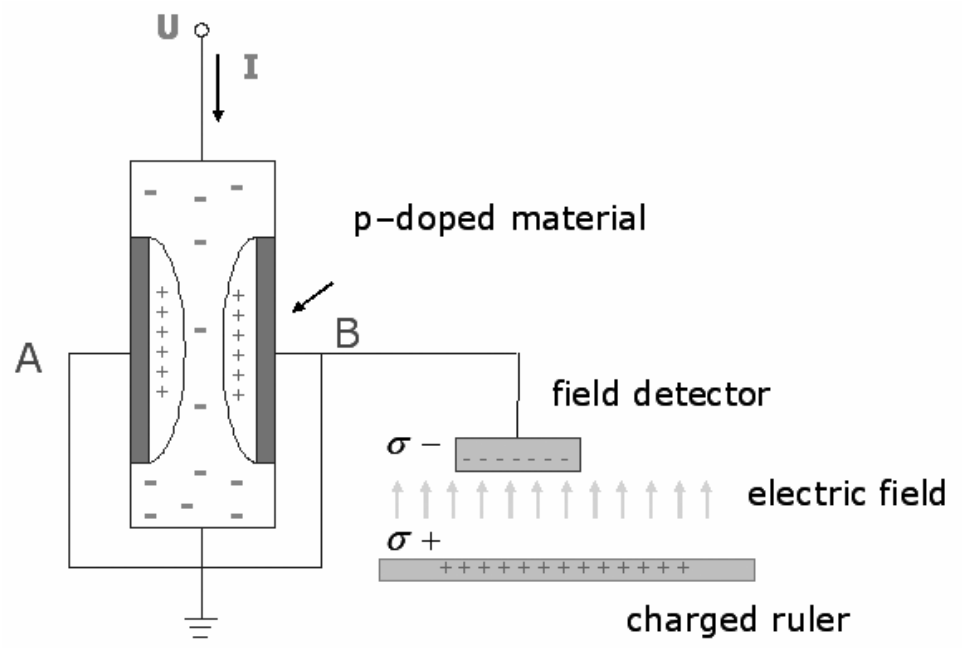


Fig.3

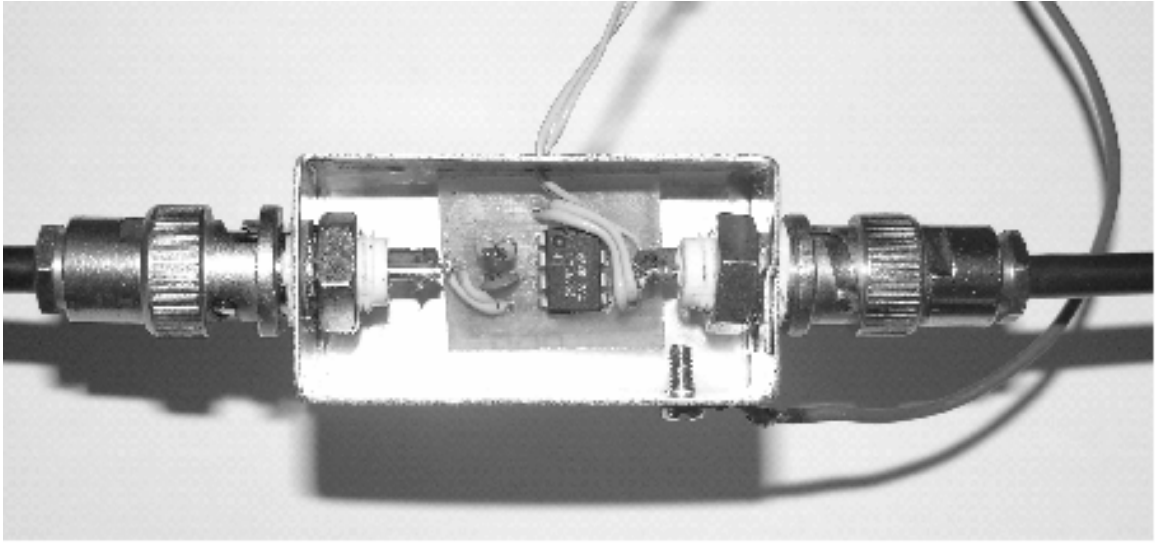


Fig.4

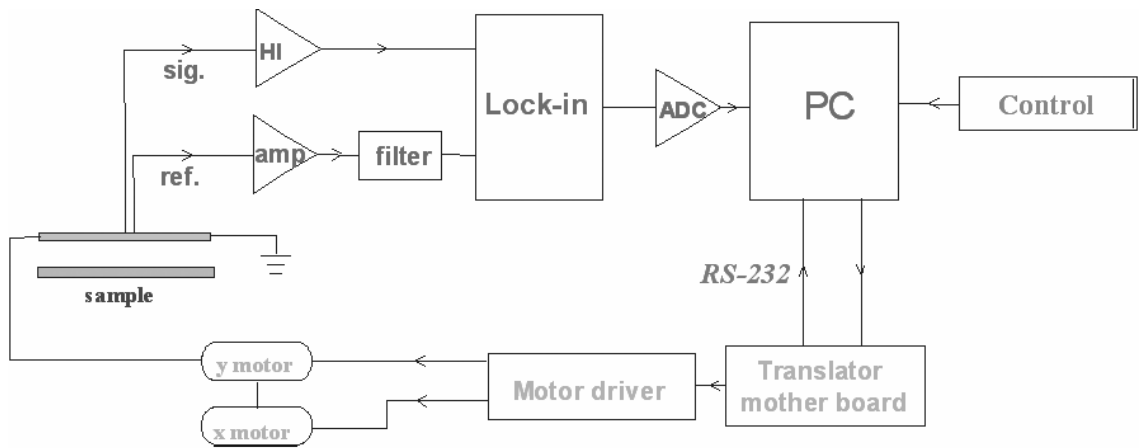


Fig.5

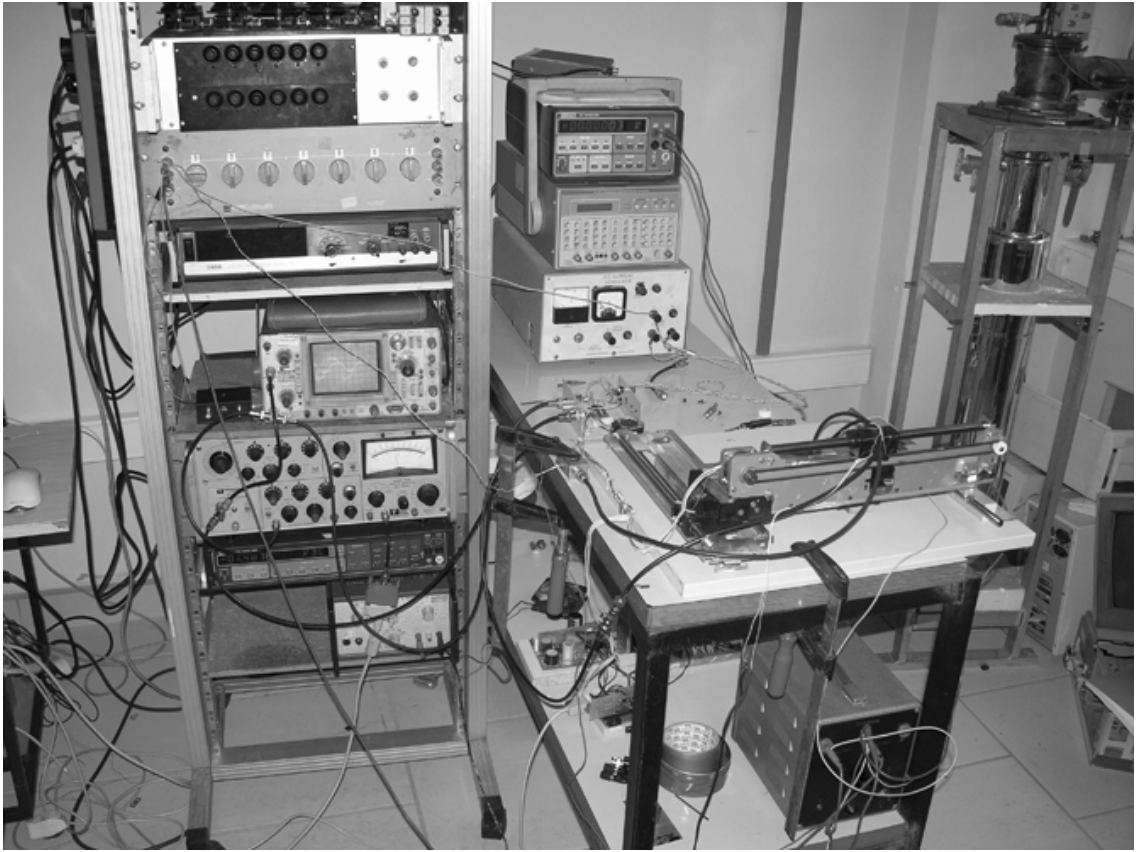


Fig. 6

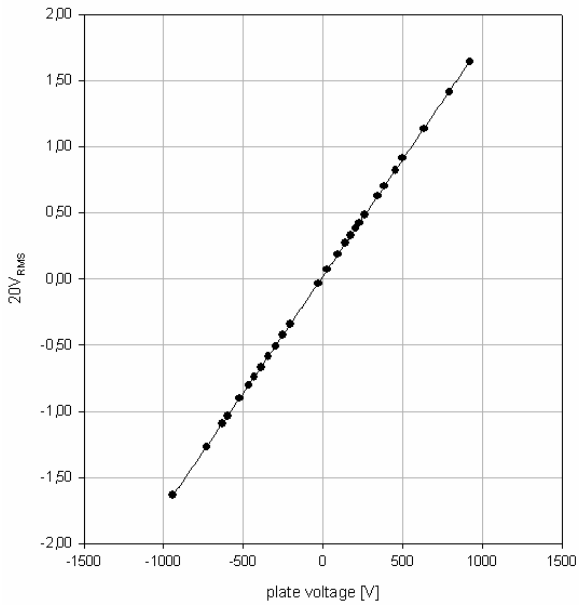


Fig.7

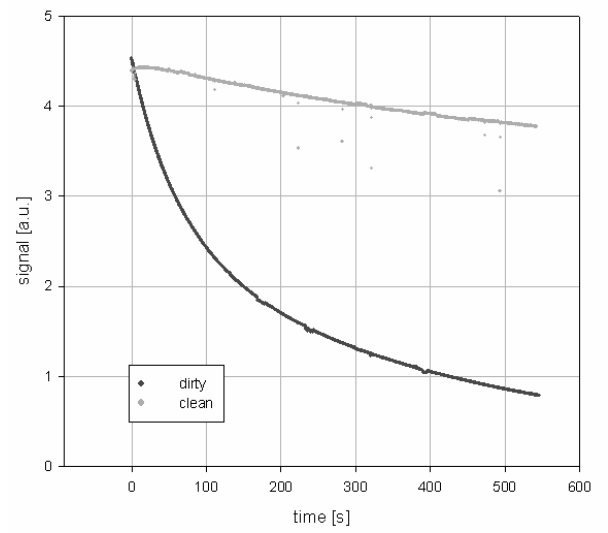


Fig. 8

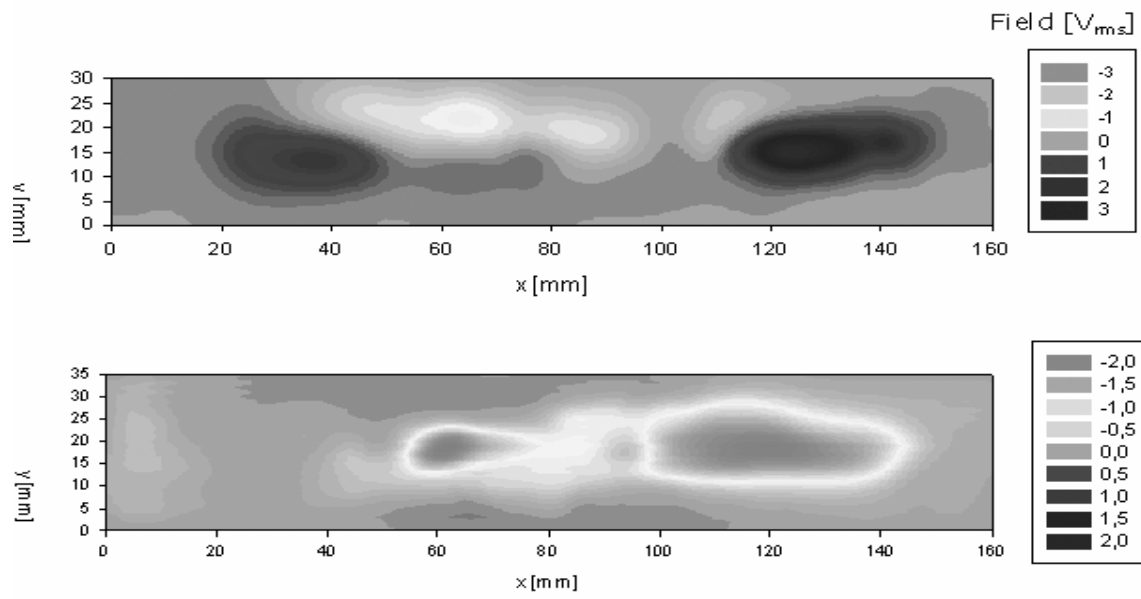


Fig.9

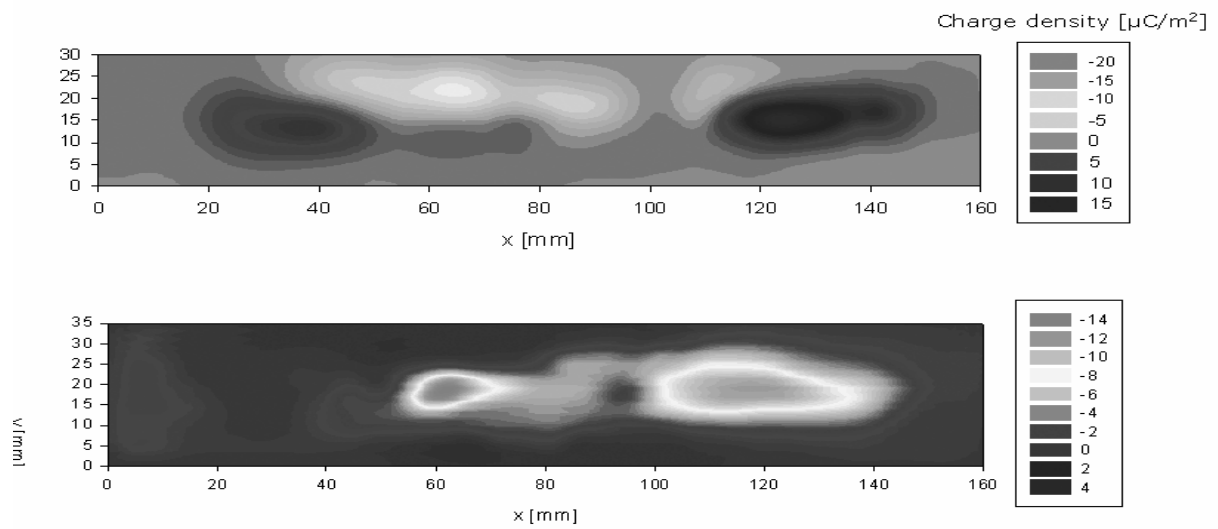


Fig.10

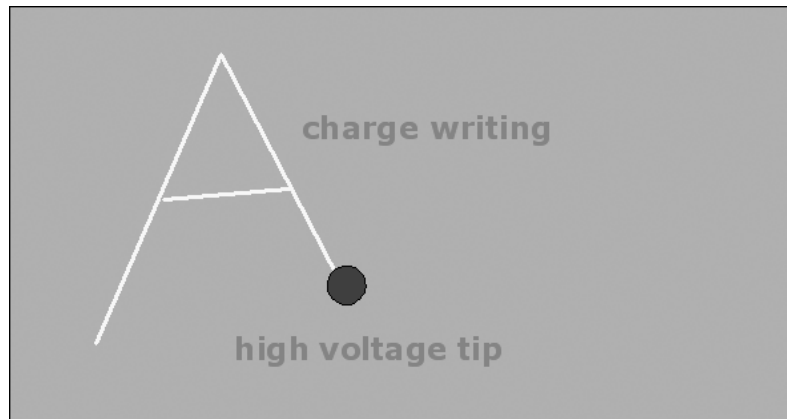


Fig.11

## 7. Problem №10: Inverted pendulum

### 7.1. Solution of Korea

#### Problem №10: Inverted pendulum

Park, Hyeongsu, Korean Minjok Leadership Academy  
1334 Sosa Anheung Hoengsung Gangwon, Korea 225-823

#### The Problem:

*It is possible to stabilize an inverted pendulum It is even possible to stabilize an inverted multiple pendulum /one pendulum the top of the other/. Demonstrate the stabilization and determine on which parameters this depends.*

This paper studies comprehensively about the methods of stabilizing an inverted pendulum. An inverted pendulum is a free hung pendulum which is upright, and just like an ordinary pendulum, it naturally falls downward because of gravity. Thus, the inverted pendulum system is inherently unstable. In order to keep it upright, or stabilize the system, one needs to manipulate it, either vertically or horizontally.

Many stabilizing methods have been developed. In 2-Dimesional system, an inverted pendulum can be stabilized thorough either vertical or horizontal oscillation with certain frequency. In 3-Dimension, rotational arms or free robot arms are used for stabilization. For algorithm, a controller using feedback system or simple oscillation both work to keep the pendulum upright, though processes or extents of stability are different from each other.

This paper first proposes theoretical background for all the cases. Then, the experiments focus on horizontal oscillation and delve into the various characteristics and factors of stabilization pattern.

## A. Physical Modeling for the Inverted Pendulum

Mechanics of the inverted pendulum is not different from that of the ordinary pendulum. It consists of a rod and a pivot. When you draw a force diagram of inverted pendulum system, it's shown as Figure 1. As seen in the diagram, force is applied to the pendulum's pivot (base).

Let  $m$  be the mass of a rod,  $P(x_0, y_0)$  coordination of the pivot,  $CM(x, y)$  coordination of the center of mass,  $l$  a distance from  $P$  to  $CM$ .

Two basic motion equations for the pendulum system are

$$m\ddot{x} = F_x, \quad m\ddot{y} = F_y - mg \quad (1)$$

and

$$I_c \ddot{\theta} = lF_y \sin \theta - lF_x \cos \theta \quad (2)$$

Where  $I_c$  is the moment of inertia of the rod with a pivot on  $CM$ .

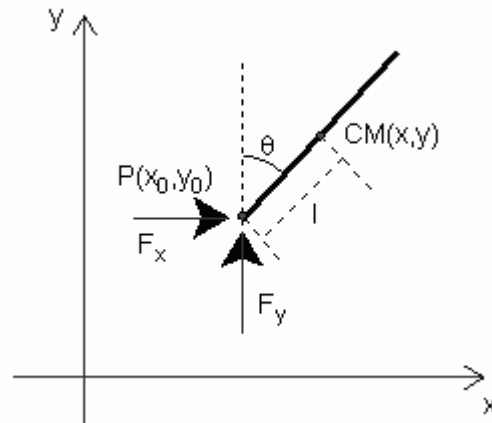


Figure 1 Force Diagram of the Inverted Pendulum

Substitute Equation (1) for  $F_x$  and  $F_y$  in Equation (2), then we obtain

$$I_c \ddot{\theta} = ml(\ddot{y} + g) \sin \theta - ml\ddot{x} \cos \theta \quad (3)$$

Then, from relationship between the coordinate of  $P$  and that of  $CM$ ,

$$x = x_0 + l \sin \theta, \quad y = y_0 + l \cos \theta \quad (4)$$

Thus,

$$\begin{aligned} \ddot{x} &= \ddot{x}_0 + l\ddot{\theta} \cos \theta - l\dot{\theta}^2 \sin \theta, \\ \ddot{y} &= \ddot{y}_0 - l\ddot{\theta} \sin \theta - l\dot{\theta}^2 \cos \theta \end{aligned} \quad (5)$$

Substitute Equation (5) for  $\ddot{x}$  and  $\ddot{y}$  in Equation (3), then the equation becomes

$$\frac{I_p}{mL} \ddot{\theta} + \ddot{x}_0 \cos \theta - (\ddot{y}_0 + g) \sin \theta = 0 \quad (6)$$

Where  $I_p = I_c + ml^2$  is the moment of inertia of the rod with a pivot on  $P$ . Equation (6) is a universal motion equation for the inverted pendulum, which can also be applied to an ordinary pendulum. This equation will be used in simulation which will be later explained. In the next chapter, we will use this equation to find stabilizing methods of the pendulum.

## B. Stabilizing Methods of the Inverted Pendulum

An inverted pendulum can be stabilized in mainly two ways: simple oscillation and feedback control system. The pendulum with oscillating base at certain frequency can stay upright without falling down. With a control system, the pendulum's movement is minutely manipulated by the machine to keep it upright.

### i) Oscillation

Oscillation is a possible method for stabilizing the inverted pendulum. Three kinds of oscillation are possible : oscillating vertically, oscillating horizontally, and rotating it. (Blitzer 1965)

#### a) The vertically driven pendulum

The inverted pendulum can be stabilized by moving it up and down at certain frequency. Mathematically,

$$x_0 = 0, \quad y_0 = A \cos \omega t \quad (7)$$

Then, Equation (6) becomes

$$\frac{I_p}{ml} \ddot{\theta} + (A \omega^2 \cos \omega t - g) \sin \theta = 0 \quad (8)$$

#### b) The pendulum driven in two dimensions

Here,  $x_0 = B \cos(\omega' t + \Phi)$ ,  $y_0 = A \cos \omega t$ . Equation (6) becomes

$$\frac{I_p}{ml} \ddot{\theta} - B \omega'^2 \cos(\omega' t + \Phi) \cos \theta + (A \omega^2 \cos \omega t - g) \sin \theta = 0 \quad (9)$$

#### c) The rotating pendulum

The rotating pendulum is the special subcase for the case two, where  $B = A$ ,  $\omega = \omega'$ ,  $\Phi = -\pi/2$ . In other words,  $x_0 = A \sin \omega t$ ,  $y_0 = A \cos \omega t$ . Then, Equation (6) becomes

$$\frac{I_p}{ml} \ddot{\theta} + A \omega^2 \sin(\theta - \omega t) - g \sin \theta = 0 \quad (10)$$

#### d) The pendulum driven horizontally

In this case,  $x_0 = A \cos \omega t$ ,  $y_0 = 0$

$$\frac{I_p}{ml} \ddot{\theta} - A \omega^2 \cos \omega t - g \sin \theta = 0 \quad (11)$$

For small oscillation,  $\theta \ll 1$ , the angle range where the inverted pendulum can be stabilized, Equation (11) is simplified into

$$\frac{I_p}{ml}\ddot{\theta} - A\omega^2 \cos \omega t - g\theta = 0 \quad (12)$$

$$\ddot{\theta} - \omega_0^2 \theta = D \cos \omega t \quad (13)$$

$$\text{where } \omega_0^2 = \frac{mgl}{I_p}, \quad D = \frac{ml\omega^2 A}{I_p}$$

In this equation  $\omega_0^2$  is remarkable because it is an angular frequency of the normal pendulum. Equation (13) is a linear differential equation, and the solution for this differential equation in terms of theta is

$$\theta = ae^{\omega_0 t} + be^{-\omega_0 t} - \frac{D \cos \omega t}{\omega^2 + \omega_0^2} \quad (14)$$

$$a = \frac{1}{2} \left[ \theta_0 + \frac{\dot{\theta}_0}{\omega_0} + \frac{D}{\omega^2 + \omega_0^2} \right] \quad (15)$$

$$b = \frac{1}{2} \left[ \theta_0 - \frac{\dot{\theta}_0}{\omega_0} + \frac{D}{\omega^2 + \omega_0^2} \right]$$

where the angular displacement and the angular velocity of the inverted pendulum at  $t=0$  is  $\theta_0$  and  $\dot{\theta}_0$ , respectively.

In order to make the pendulum oscillate, the exponentially increasing term, or the exponential term with a positive exponent, should be eliminated. Thus,  $a$  should be equal to zero, or

$$\dot{\theta}_0 = -\omega_0 \theta_0 - \omega_0 \frac{D}{\omega^2 + \omega_0^2} = -E\omega_0 \quad (16)$$

$$\text{where } E = \theta_0 + \frac{D}{\omega^2 + \omega_0^2}$$

Then, the final solution for theta becomes

$$\theta = Ee^{-\omega_0 t} - \frac{D \cos \omega t}{\omega^2 + \omega_0^2} \quad (17)$$

When  $t$  approaches to infinity, theta converges to

$$\theta = -\frac{D \cos \omega t}{\omega^2 + \omega_0^2} \quad (18)$$

To conclude, when the pendulum's pivot oscillates in  $x_0 = A \cos \omega t$ ,  $y_0 = 0$ , it can be

stabilized with  $\theta = -\frac{D \cos \omega t}{\omega^2 + \omega_0^2}$ . Although theta does not converge into one value, it does

keep upright while oscillating constantly. The experiments, which will be explained later, focus on the relationship between  $x_0$  and theta.

## ii) Feedback Control system.

Another method to stabilize the inverted pendulum is using feedback control system. Feedback control system is the process in which the movement of the pendulum's pivot is continuously fed back based on the pendulum's physical condition in order to keep the pendulum upright. For example, at one moment, when the pendulum leans to the right, the base moves fast to the right so that the pendulum becomes upright. Still, the base should move in a

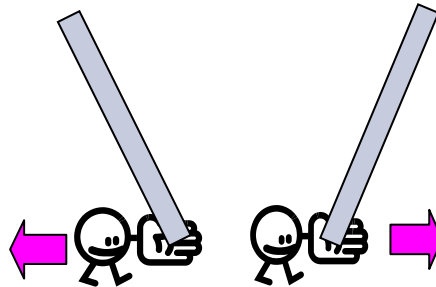


Figure 2 Fundamentals of how the inverted pendulum is stabilized  
**Purple arrows indicate the direction toward which the inverted pendulum should move when it is leaned as shown above.**

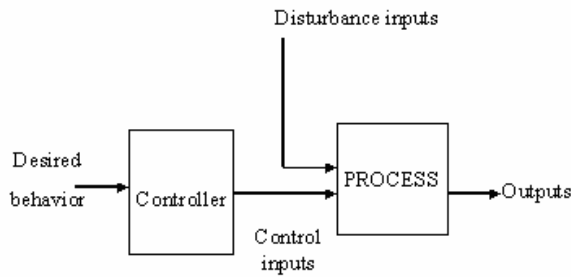
certain force because either too fast motion or too slow motion fails the stabilization. When it starts to lean to the left, the pendulum's base moves left to make it upright again.

In definition, feedback control system monitors certain output of the system and manipulates its inputs to keep the output near to desired value. As seen in Figure 3, it is also called closed loop control system because the output affects the input which again produces the next output, repeating the cycle. It has several advantages over an open-loop controller it can quickly respond to the possible disturbances or uncertainties and keep the pendulum stabilized constantly.

In the closed loop controller, the desired output is called the reference. Difference between the reference and the current output is the error. The objective of the feedback control system is making it zero by manipulating inputs of the system. The diagram for feedback control system is shown as below.

In the case of the inverted pendulum,  $x$ , the position of the inverted pendulum, and  $\theta$ , an angle between the rod and the perpendicular line, are outputs. Desired behavior, or reference, is  $\theta = 0$ ; we want to keep it upright. Their values are measured by instruments and put into the controller to calculate an input. The input is the force applied to the base of the pendulum, through which we manipulate its movement. However, the disturbance inputs, such as mechanical frictions, also involves in the motion of the inverted pendulum (Process), along with the input from the controller. Then,  $x$  and  $\theta$  change, and these outputs again are measured and put into controller, completing one revolution of a closed-loop control system.

### Open Loop Control System



### Closed-Loop (a.k.a FEEDBACK) Control System

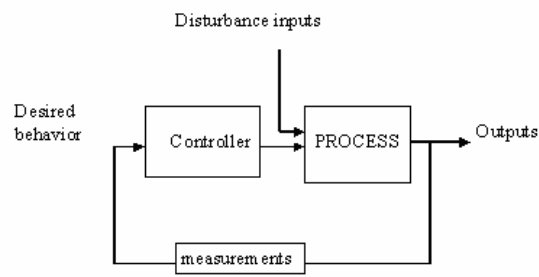


Figure 3 Comparison between Open Loop Control System and Closed Loop Control System<sup>1</sup>

**Feedback control system differs from open loop system because it measures the output and feedback it to the controller. Output determines the value of the next output.**

Among many kinds of controllers, a PID controller is a common feedback loop system. PID stands for Proportional, Integral, and Derivative. As the name implies, the input of the system is determined by three variations of the output's value; the error (Proportional), integral value of the error (Integral), derivative value of the error (Derivative). The equation for PID controller is shown as below.

$$Output = P + I + D$$

$$= K_p \cdot e + K_I \cdot \int e \cdot dt + K_D \frac{de}{dt} \quad (19)$$

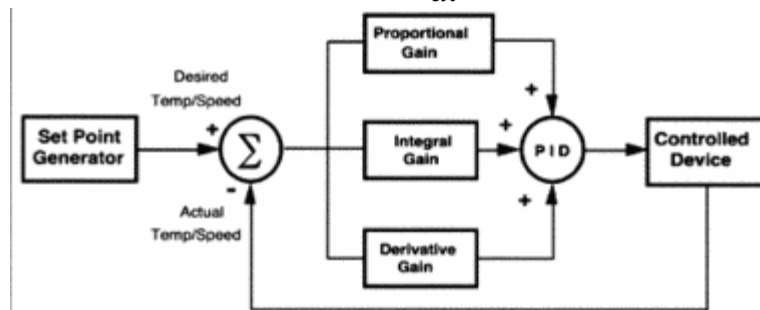


Figure 4 Diagram for PID Controller<sup>2</sup>

PID controller uses proportional gain, integral gain, and derivative gain of the error in order to determine the value of output which can make the error zero

This equation is needed to be analyzed in each component in physical points of view. In the inverted pendulum system, the error signifies how much the pendulum leans.

<sup>1</sup> <http://www.ic-tech.com/Fuzzy%20Logic/>  
(Diagram 1: open 2: general 3. specified)

<sup>2</sup> <http://www.brewerscience.com/products/cee/technical/ceepid/>

### a) Proportional component

The error is multiplied by  $K_p$  and added to the controlled output. For example, for a heater, a controller with a proportional band of  $10\text{ }^\circ\text{C}$  and a setpoint of  $20\text{ }^\circ\text{C}$  would have an output of 100% at  $10\text{ }^\circ\text{C}$ , 50% at  $15\text{ }^\circ\text{C}$  and 10% at  $19\text{ }^\circ\text{C}$ .<sup>3</sup>

In the pendulum system, when the rod leans more, the increased theta increases the sum of output. The result is that more force is applied to the pendulum's base. Note that when the error is zero, a proportional controller's output is zero.

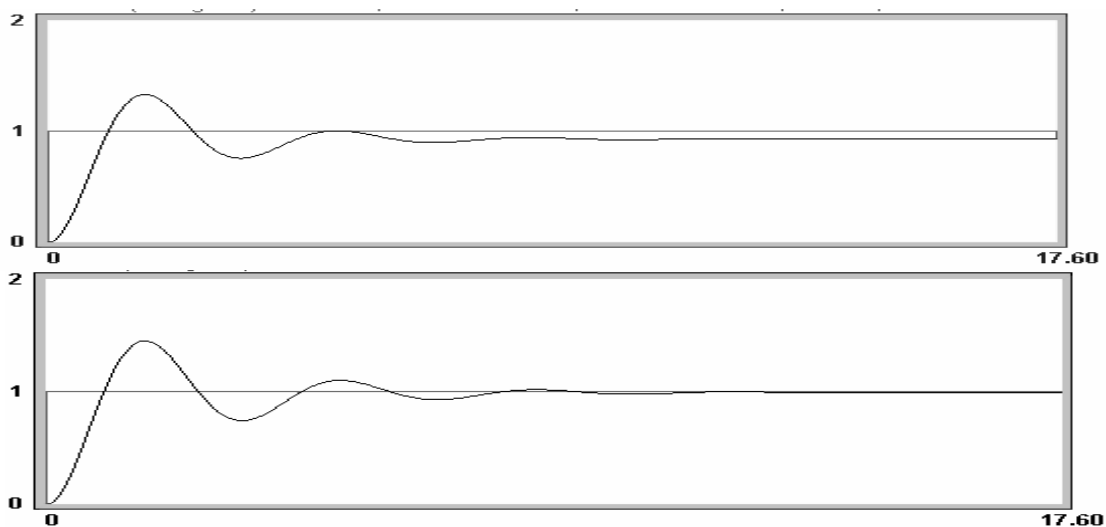
### b) Integral component

Integral component signifies the average error during pendulum's movement. Integral movement extenuates too fast response from P and D components. From balance between I component and P/D component, the PID controller determines the patterns of stabilization.

### c) Derivative component

Derivative of the error, or theta, is an angular velocity omega of the pendulum. It signifies how fast the pendulum is falling. The faster it falls, the more the force applied to it should be.

Each component contributes differently to the stabilization. Increase in proportional coefficient causes fast response, but it causes overshoots and steady state errors. Overshoots mean unnecessarily overt reaction. The highly responsive pendulum exerts too much force that the pendulum goes over the perpendicular line and fall down out of control. Also, steady state error is an error which is not removed by the controller. Bad controllers don't make error zero, and the value the error converges is steady state error. The integral component has a force which eliminates this steady state error. Although large value of integral gain may make oscillations even larger and make the system unstable, reducing the error improves the accuracy of the system. Lastly, derivative component also contributes to fast reaction and, more importantly, provides a dampening effect to eliminate oscillation and overshoots. In the inverted pendulum system, it provides an overall stability to it.



<sup>3</sup> Wikipedia : PID Controller

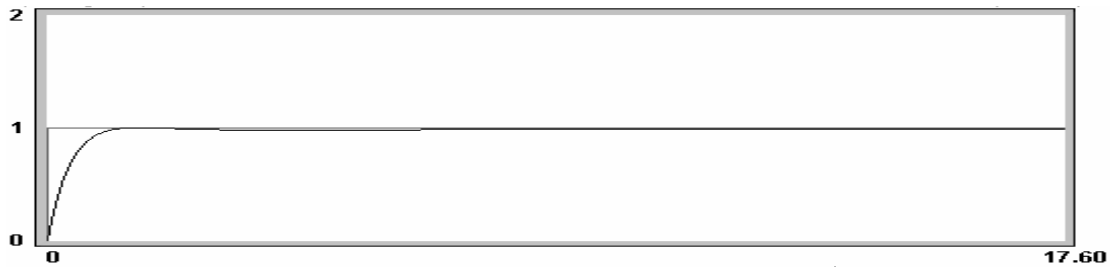


Figure 5 P Control, PI Control, PID Control (from top to bottom)<sup>4</sup>

**P component is basic measure of the control system, I component eliminates steady state error, and D component extenuates oscillation.**

Since each component has its good and bad points, one should combine the three in order to make the best stabilization of the pendulum. Finding ideal PID coefficients will be later explained in Discussion section.

### **iii) Difference between the two methods.**

Both oscillation and feedback system can stabilize the inverted pendulum. However, their characteristics are different each other. In their mechanisms, simple oscillation is a kind of open-loop controller, whose input is fixed at any time. In contrast, feedback system is a complicated system whose input continuously changes depending on the pendulum's physical condition. As a result, it's unable to exactly predict the pendulum's motion.

The differences in physical complexity also determine the differences in the controlling device. Oscillating the pendulum needs a very simple machine such as a robot arm or a speaker (which makes very minute oscillations), but to realize feedback system needs an advanced electrical device which can perform differentiation and integration, and simulate mathematical modeling.

Nevertheless, feedback system is not an inefficient controller. Rather, the opposite is true. Complexity of the PID controller enables very flexible control compared to oscillation. In a strict sense, oscillating imperfectly stabilizes the pendulum because it doesn't make the rod stand upright but oscillate continuously. However, PID controller can vary the stabilizing movement by manipulating the values of P, I, D gains. In one case, one can make the stabilized pendulum oscillating precariously. In the other, one can make it exactly upright and not moving a bit.

**Table 1 Comparison between oscillation and feed back control system**

	Cost	Instruments	Complexity	Flexibility
Oscillation	Less	Simple(speaker)	Can be solved with a clear-cut motion equation	Only one can stabilize or not.
Feedback System	More	Complex (a device with complicated arithmetic calculation)	Nonlinear Need to be familiar with control theory	Can vary the pattern of stabilization

<sup>4</sup> Cuthbert Nyack Control (<http://controlcan.homestead.com/files/acontrol/con2pid.htm>)

### C. Apparatus

Realizing the control system needs computer program which can simultaneously check the pendulum's conditions and calculate.

The inverted pendulum moves by the cart attached to it. The cart is fixed on a screw rail run by a motor. The cart and the pendulum do not move itself but the rail does. The motor is connected to the computer and it takes in charge of all the calculations needed for a PID controlling. The computer receives the information of  $x$  and  $\theta$ , calculates how much force is needed to make the pendulum upright, and gives the value for torque applied to the motor. The motor's speed is determined by at every one thousandth second. Using CEMTool, a Matlab based program for controlling, we constructed PID controller system, which measures  $x$  and  $\theta$  and calculates the force applied to the cart at every 0.001s.

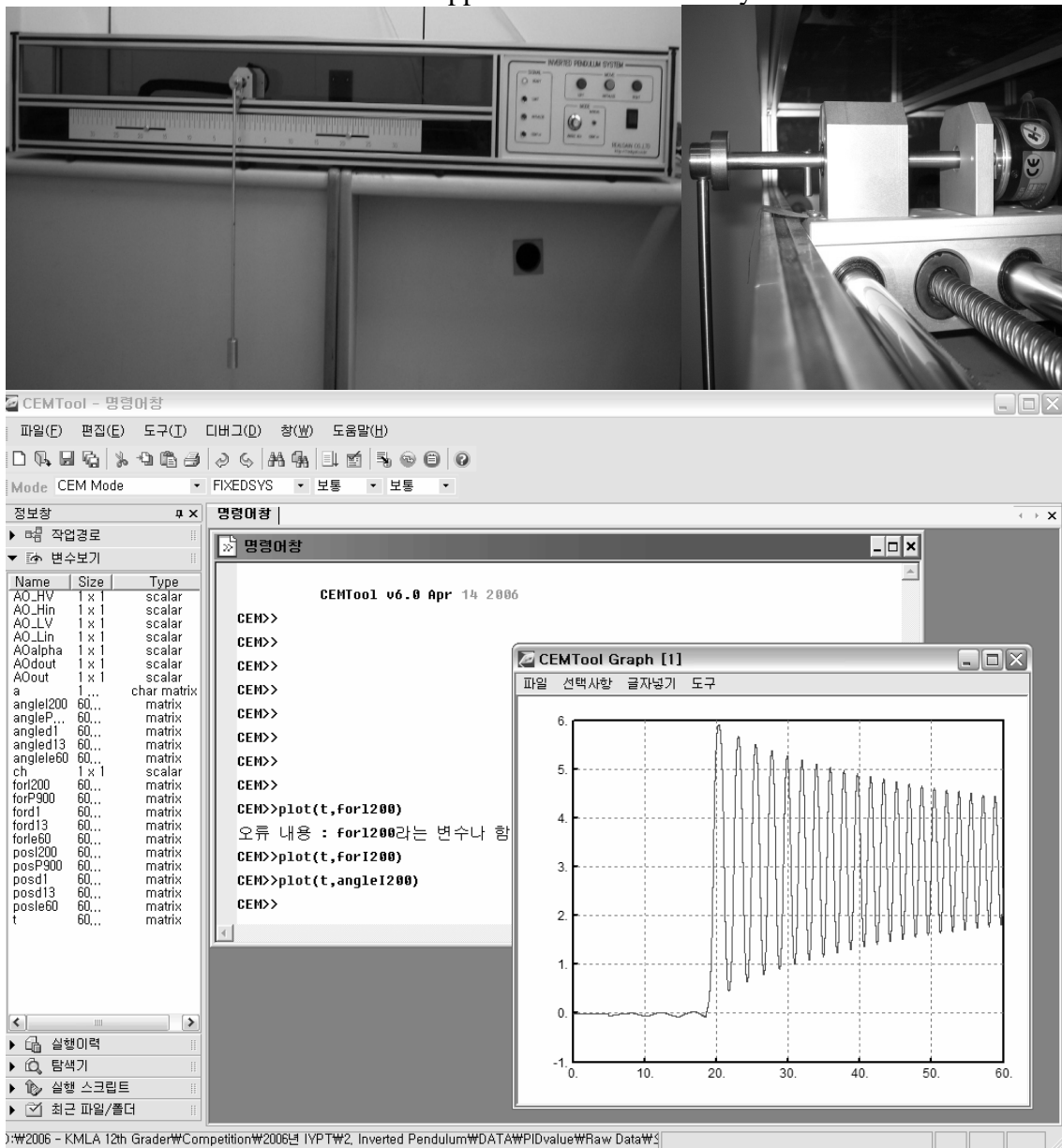


**Figure 6 Apparatus of the Experiments (upper column) and Interface of CEMTool (lower column)**

## D. Experimental Method

Because of the limitation in the apparatus, we made experiments only on the case I and case iii.

### i) horizontal oscillation

To realize the horizontal oscillation of the pendulum, we should know which function of the force is needed to make the pendulum oscillate precisely. However, the mechanics of the inverted pendulum system is complicated by the cart, the rail, and the motor which are not considered in the theoretical model. The precise physical model which takes those three into account is shown in Equation 20 & 21.

$$F = (m + M)\ddot{x} + b\dot{x} + ml\ddot{\theta} \cos\theta - ml\dot{\theta}^2 \sin\theta \quad (20)$$

$$-\ddot{x} \cos\theta - g \sin\theta = 2l\ddot{\theta} \quad (21)$$

Basically, the real physical model has nonlinear components, so it's unable to get a solution for force F to make  $x_0 = A \cos \omega t$ ,  $y_0 = 0$

As a result, we needed to adopt PID controller in order to realize the horizontal oscillation. By handling PID gains, we made the pendulum stabilize with oscillation, and then began experiments. Although the process of setting the gains' values is arbitrary because of the system nonlinearity, we were able to vary the stabilization patterns using a conventional method for setting PID gains without mathematical calculation.<sup>5</sup>

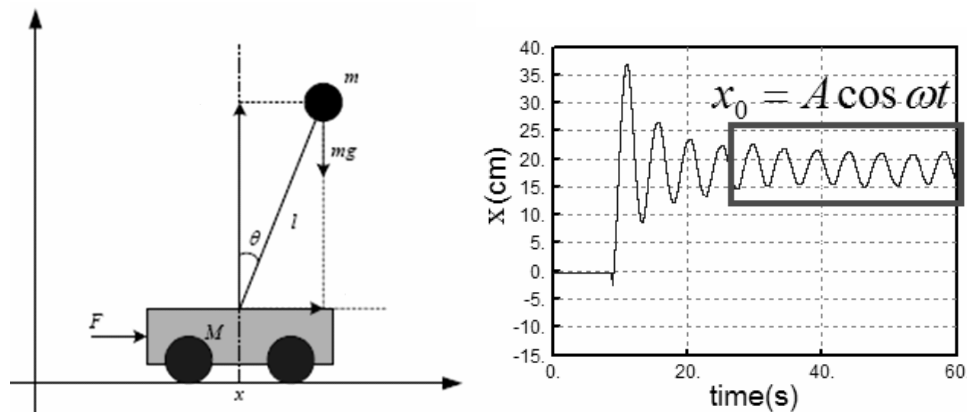


Figure 7 Diagram of cart-pendulum system (Left) and Oscillation interval of the controlled inverted pendulum (Right)

### a) Experiment 1 : Proving the theory's validity

In the theoretical background part, we proved that in the stabilizing pendulum the value of theta is determined by x. From the graph of x, we drew the graph of theta calculated from Equation (18). Then, it is compared with the experimental value.

---

<sup>5</sup> Engineers in the control theory use more complicated method to determine PID gains, but we didn't use it because this paper focuses on the motion of the inverted pendulum, not the PID controller itself.

**b) Experiment 2 : how mass and length affect stabilization**

Among many variables which affect the stabilization of the inverted pendulum, its mass and length greatly determine major part of its motion, like those of the free-falling pendulum.

The pendulum consists of the heavy weight at the end and the rod. We prepared 4 different finds of weights (24.4g, 35.9g, 73.3g, 108.5g) and observed the difference in stabilizing pattern. Then again, with 4 different kinds of rods (30cm, 40cm, 60cm, 70cm) the experiments were repeated.

**ii) Experiment 3 : PID Control**

As mentioned before, with PID controller the inverted pendulum can have various stabilized patterns. It is also possible to stabilize faster and more accurately than simple oscillation. In this experiment, we searched for the condition of PID coefficients which can achieve the perfect stabilization of the inverted pendulum.

First, we changed the values of PID coefficients one by one and checked their effects each. In this case, we decided the standard of perfect stabilization as followings: first, less time to reach stabilization (less than 5 seconds) and, second, almost no oscillation after stabilization (angular amplitude less than 1cm). First, through simulation using CEMTool, we first grasped the range of PID coefficients which stabilizes the pendulum. Then, minute adjustment was based on actual demonstrations.

**E.Result**

**i) Experiment 1 : validity of the theory**

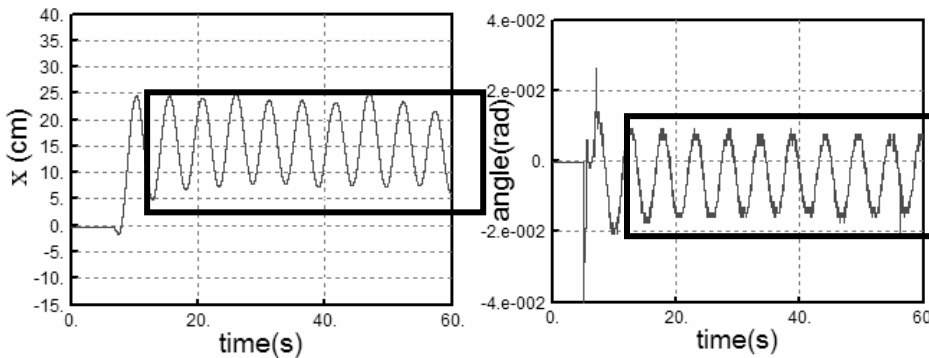


**Figure 8 Graph of x and theta of the inverted pendulum stabilized by PID Controller**

Black box shows the oscillating interval.

It was previously mentioned that when the inverted pendulum is imposed an oscillation  $x_0 = A \cos \omega t$ ,  $y_0 = 0$ , theta becomes  $\theta = -\frac{D \cos \omega t}{\omega^2 + \omega_0^2}$ . Figure 8 is graphs for  $x_0$  and theta measure from Experiment 1, and we can see that when x starts to follow a sinusoidal function, theta also resembles a sinusoidal function, implying the validity of the theoretical model. To prove that the the function of theta is exactly the same with that calculated by theoretical model, we should check the amplitude and angular frequency of the cosine fuction. Table 2, shown below, is the result for the comparison of angular frequency at various lengths and

masses. Notice that length of the pendulum, shown in the table, is equal to L, not l, which is defined as the distance between the pendulum's pivot and the pendulum's center of mass. The relationship between L and l is later calculated in Appendix 1. m is the mass of the weight attached at the end of the pendulum.

**Table 2 Comparison of Experimental Value and Theoretical Value of Angular Frequency**

L (cm)	30	40	60	70
m (g)	108.5	108.5	108.5	108.5
$\omega_{\text{exp}}$	1.213 $\pm 0.081$	1.206 $\pm 0.040$	1.230 $\pm 0.061$	1.206 $\pm 0.053$
$\omega_{\text{theory}}$	1.199	1.220	1.199	1.215
Error	0.014	0.014	0.031	0.009
L (cm)	40	40	40	40
M (g)	24.4	35.9	73.3	108.5
$\omega_{\text{exp}}$	1.188 $\pm 0.060$	1.213 $\pm 0.051$	1.236 $\pm 0.063$	1.239 $\pm 0.062$
$\omega_{\text{theory}}$	1.198	1.207	1.218	1.229
Error	0.01	0.006	0.018	0.01

**Table 3 Comparison of Experimental Value and Theoretical Value of Angular Amplitude**

L (cm)	30	40	60	70
m (g)	108.5	108.5	108.5	108.5
$\theta_{\text{exp}}^0$	11.257 $\pm 0.909$	7.068 $\pm 0.785$	5.498 $\pm 0.785$	5.149 $\pm 1.277$
$\theta_{\text{theory}}^0$	11.596	7.221	6.049	4.633
Error	0.339	0.153	0.551	0.516
L (cm)	40	40	40	40
m (g)	24.4	35.9	73.3	108.5
$\theta_{\text{exp}}^0$	19.350 $\pm 0.785$	17.618 $\pm 0.453$	12.043 $\pm 0.906$	6.977 $\pm 0.453$
$\theta_{\text{theory}}^0$	19.984	18.070	11.865	7.427
Error	0.634	0.402	0.178	0.450

The error between expected amplitude and actual amplitude and that between expected frequency and actual frequency are little. From the result, we can see that the theoretical

model fits well with the actual experiment. Finally, when the pendulum's pivot oscillates

in  $x_0 = A \cos \omega t$ ,  $y_0 = 0$ , it can be stabilized with theta  $\theta = -\frac{D \cos \omega t}{\omega^2 + \omega_0^2}$ .

## ii) Experiment 2 : how mass and length affect stabilization

So far, we saw that the theoretical model for the inverted pendulum is correct by comparing theoretical estimates and experimental values. Next, how the pendulum's physical characteristics, such as length and mass, affect the pattern of stabilization is studied during Experiment 2.

Figure 9 shows the result. For every length of the rod, a weight with 108.5g was used. As longer rod is used, the amplitude of the oscillation decreases while frequency keeps the same value.

Also, we varied the mass of the weight on the tip of the pendulum. For every mass of the rod, a 40-centimeter-long rod is used. As a weight with heavier mass is used, the amplitude of the oscillation decreases while frequency keeps the same value. One with a heavier mass tends to be stable.

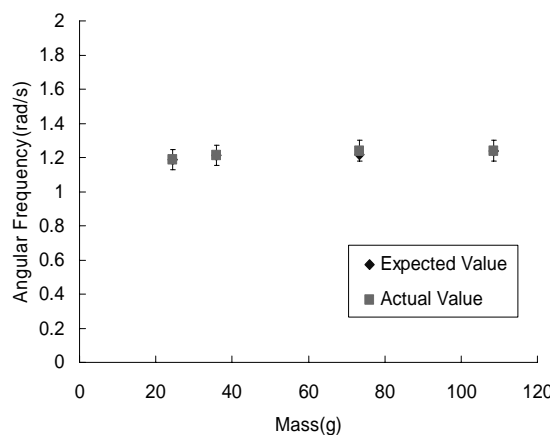
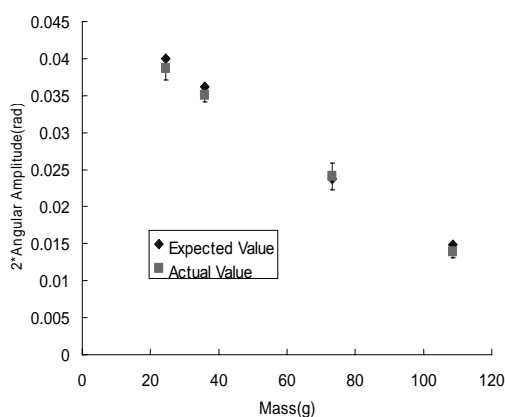
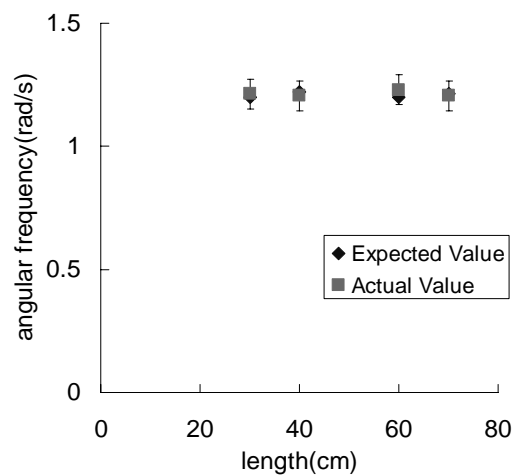
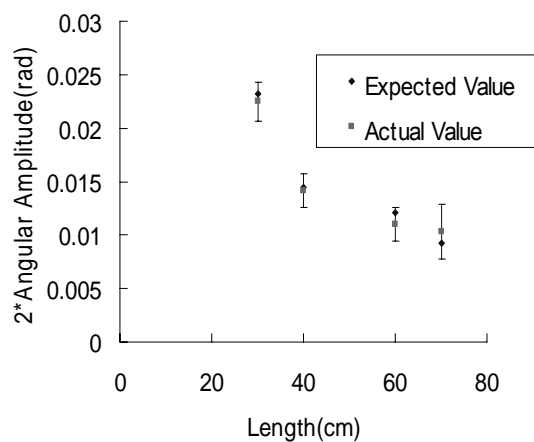


**Figure 9 Effects of Mass and Length**

As length increases, the amplitude of the cosine function decreases while the frequency remains the same. In other words, the long pendulum stabilizes more readily.

### iii) Experiment 3 : PID Controller

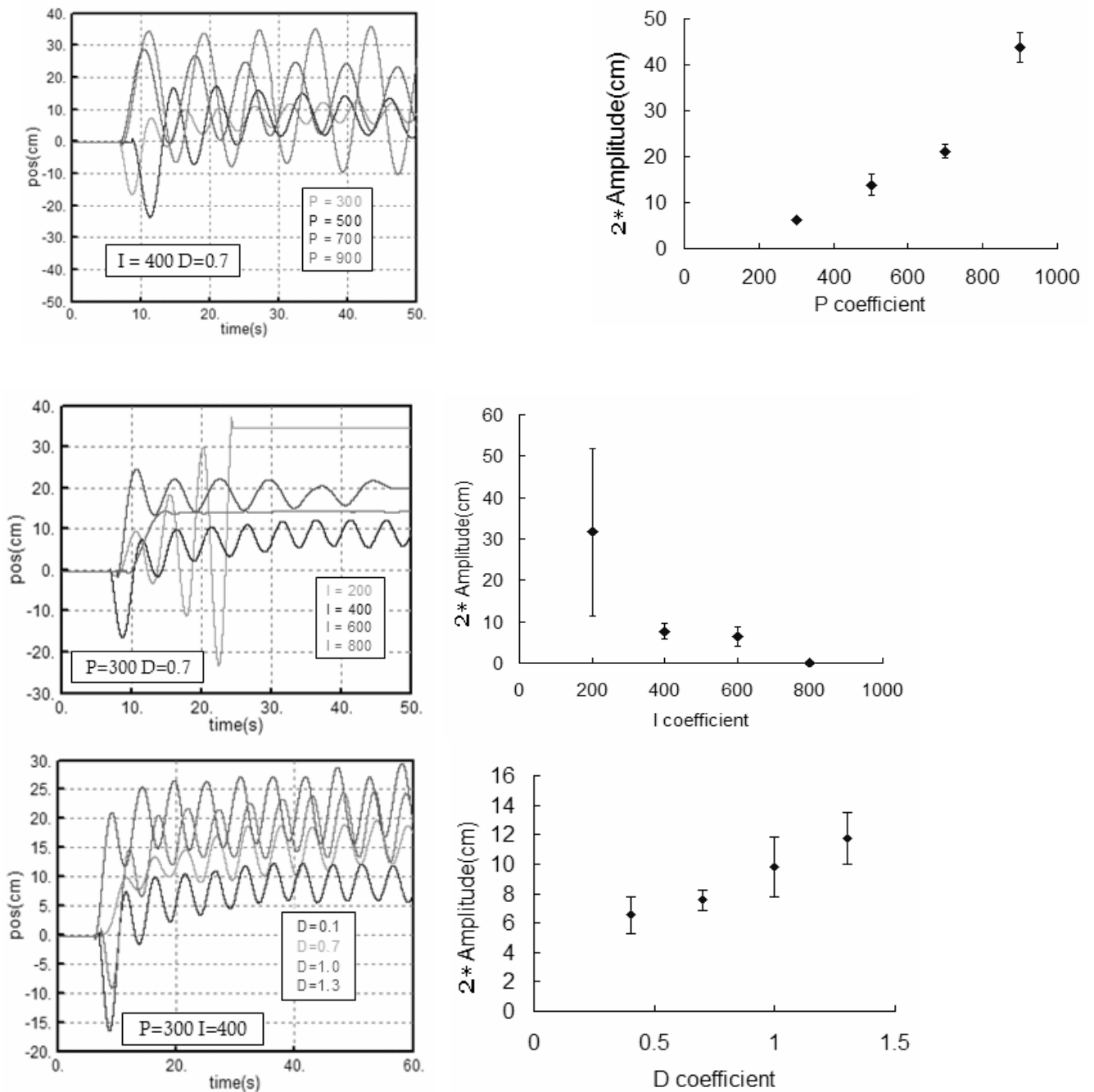


**Figure 10 Effects of P, I, D Coefficients**

Figure 10 shows how the pendulum's movement changes with P, I, D coefficients. Although the only obvious characteristic shown in the graph is amplitude, it still represents the coefficients' roles in stabilization. As P increases, the amplitude increases, which is very characteristic of P component. As I increases, the amplitude recognizably decreases, and especially when I = 800, the pendulum is stabilized with almost no oscillation. This case (P=300, I = 800, D=0.7) fits to the conditions of perfect stabilization. As D increases, the amplitude increases. Difference between P and D is that the amplitude changes a lot more by D than by P. The next chapter will analyze the result from the two experiments.

## F. Discussion

### i) Experiment 2 : length

$$\begin{aligned}
 A_{ang} &= \frac{D}{\omega^2 + \omega_0^2} \\
 &= ml\omega^2 A / (I\omega^2 + mgl) \\
 &= m\left(\frac{2M+m}{2M+2m}\right)L\omega^2 A / \left(\left(M + \frac{1}{3}m\right)L^2\omega^2 + mg\left(\frac{2M+m}{2M+2m}\right)L\right) \\
 &= \frac{\alpha L}{\beta L^2 + \gamma L} = \frac{\alpha}{\beta L + \gamma} \tag{22}
 \end{aligned}$$

where L is the length of the pendulum, l the distance between its pivot and its center of mass, m mass of the rod, M mass of the weight.

Substituting m, M, l,  $\omega^6$  for D and  $\omega_0$  clearly explains more stable motion in the longer pendulum. As seen in the last Equation (22), L is in the denominator so that increase in L eventually results in decrease in angular amplitude

In viewpoint from energy and torque, more length means more moment of rotation. Thus, the rotational energy from the basis affects less to the end of the long pendulum than that of the short pendulum. It results in less overshoots, making the pendulum more stable.

Constancy of the angular frequency is because angular frequency of theta is the same with frequency of x, defined by  $\omega$ . Thus, length does not affect to the frequency. Note that the free falling pendulum's frequency is affected by length.

### ii) Experiment 2 : mass

$$A_{ang} = m\left(\frac{2M+m}{2M+2m}\right)L\omega^2 A / \left(\left(M + \frac{1}{3}m\right)L^2\omega^2 + mg\left(\frac{2M+m}{2M+2m}\right)L\right) \tag{23}$$

From equation (23), increase in M causes angular amplitude decreases as denominator increases faster than numerator.<sup>7</sup> Thus, the graph in Figure 9 supports the theoretical expectation.

### iii) Experiment 3 : PID Controller

The result from Experiment 3 basically supports the characteristics of P, I, D gains. Increase in P and D coefficients makes the response faster at cost of stability. As a result, the angular amplitude increases as the coefficients become larger. On the other hand, I coefficient improves the stability of the inverted pendulum system and reduces its angular amplitude.

We also saw the one case of perfect stabilization, in which the pendulum is stabilized with almost no oscillation. To find such cases of perfect stabilization, there are various methods, such as Ziegler-Nichols auto-tuning method and Relay auto-tuning method. However, in most cases, they are based not on physical modeling but mathematical control

<sup>6</sup> Detailed procedure of substitution is shown in the appendix 2.

<sup>7</sup> Detailed explanation for this statement is shown in the appendix 3.

theories. Although there are model-based methods such as root-locus method and transient response method, they are hard to apply to the inverted pendulum system because of its complexity. As explaining about the methods need comprehensive knowledge of control theories, we just introduce the name of methods.

## G. Conclusion

The paper covers the inverted pendulum and its various controlling methods, including PID controller. Theoretical model was established based on the basic mechanism of the ordinary pendulum, and proved true by a series of experiments. It also enables us the prediction for how physical characteristics of the pendulum, such as mass and length, affects its movement and stability. The experiments showed the valid relationship between the pendulum's physical traits and stabilization patterns, which also correspond to the theoretical expectation. Finally, PID controller provides the possibility that the pendulum can not only just be stabilized but also be stabilized with various patterns. Among them, we analyzed the perfect stabilization case and realized it. In this aspect, PID controller shows high applicability and flexibility in controlling the inverted pendulum.

For one who should choose between PID controller or simple oscillation, the choice depends on one's preferences. As those two methods have strengths and weaknesses, shown in Table 1, one should choose strong points as a tradeoff for other strengths. In conclusion, the question how to keep the pendulum upright has many answers, and the choice is open to the users.

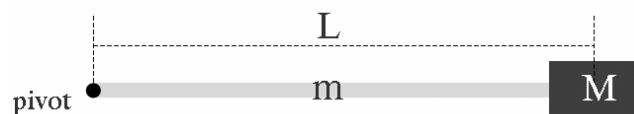
## Bibliography

- [1] Blitzer, L. "Inverted Pendulum." American Journal of Physics, Volume 33, Issue 12, June 1965, pp.1076-1078.
- [2] Fuzzy Control Methods and their Real System Applications Presented by IC Tech, Inc., April 2000 URL: <http://www.ic-tech.com/Fuzzy%20Logic/>
- [3] PID Control, Brewer Science, URL: <http://www.brewerscience.com/products/cee/technical/ceepid/>
- [4] Wikipedia : PID Controller. URL: [http://en.wikipedia.org/PID\\_Controller](http://en.wikipedia.org/PID_Controller)

PID제어기 계수는 제어대상 시스템의 모델이 주어질 경우에 주파수영역 설계법, 근궤적법 등을 사용하여 반복과정을 통해 설계할 수 있다.

## Appendices

### i) Calculation of the Center of Mass and Rotational Inertia



**a) Center of Mass**

$$l = x_{CM} = \frac{\frac{1}{2}L \cdot m + L \cdot M}{m + M}$$

$$= \frac{2M + m}{2M + 2m} L$$

**b) Rotational Inertia**

$$I = I_{rod} + I_{mass}$$

$$= \frac{1}{3}mL^2 + ML^2$$

$$= \left(\frac{1}{3}m + M\right)L^2$$

**ii) Detailed process of the equation for angular amplitude**

$$A_{ang} = \frac{D}{\omega^2 + \omega_0^2}$$

where  $\omega_0^2 = \frac{mgL}{I_p}$ ,  $D = \frac{mL\omega^2 A}{I_p}$ ,  $I = \left(\frac{1}{3}m + M\right)L^2$

When we all substitute  $\omega_0$ , D, and I, the equation becomes

$$A_{ang} = \frac{D}{\omega^2 + \omega_0^2}$$

$$= \frac{\frac{ml\omega^2 A}{I}}{\omega^2 + \frac{mgl}{I}}$$

$$= ml\omega^2 A / (I\omega^2 + mgl)$$

$$= m\left(\frac{2M + m}{2M + 2m}\right)L\omega^2 A / \left(\left(M + \frac{1}{3}m\right)L^2\omega^2 + mg\left(\frac{2M + m}{2M + 2m}\right)L\right)$$

$$= \frac{\alpha L}{\beta L^2 + \gamma L} = \frac{\alpha}{\beta L + \gamma}$$

where  $\alpha = m\left(\frac{2M + m}{2M + 2m}\right)\omega^2 A$ ,  $\beta = \left(M + \frac{1}{3}m\right)\omega^2$ ,  $\gamma = mg\left(\frac{2M + m}{2M + 2m}\right)$

**iii) Denominator and numerator of the angular amplitude**

The objective is to determine which side, denominator or numerator of the angular amplitude, increases faster as M increases.  $\omega$  and A have their maximum value because the inverted pendulum cannot be stabilized over certain value of  $\omega$  and A. Although the

thresholds cannot be measure precisely, the experiments showed that approximate maximum value for  $\omega$  and A is 1.5 and 0.3, respectively. Thus,

$$\omega^2 A < 1.5^2 * 0.3 < g \approx 9.8$$

Multiply the both sides by mL, then,

$$mL\omega^2 A < mgL$$

Thus, when x is variable,  $mL\omega^2 Ax$  increases faster than  $mgLx$ . When

$$x = \frac{2M + m}{2M + 2m}, m\left(\frac{2M + m}{2M + 2m}\right)L\omega^2 A \text{ increases faster than } mg\left(\frac{2M + m}{2M + 2m}\right)L \text{ as } x \text{ increases.}$$

$$\text{Also, } mg\left(\frac{2M + m}{2M + 2m}\right)L < \left(M + \frac{1}{3}m\right)L^2\omega^2 + mg\left(\frac{2M + m}{2M + 2m}\right)L.$$

Thus,  $m\left(\frac{2M + m}{2M + 2m}\right)L\omega^2 A$  increases faster than  $\left(M + \frac{1}{3}m\right)L^2\omega^2 + mg\left(\frac{2M + m}{2M + 2m}\right)L$  as x increases

$$\text{Since } x = \frac{2M + m}{2M + 2m} = 1 - \frac{m}{2M + 2m}, \text{ x increases as M increases.}$$

Thus,  $m\left(\frac{2M + m}{2M + 2m}\right)L\omega^2 A$  increases faster than  $\left(M + \frac{1}{3}m\right)L^2\omega^2 + mg\left(\frac{2M + m}{2M + 2m}\right)L$  as M increases

In other words, the denominator of  $A_{ang}$  increases faster than the numerator of  $A_{ang}$  as M increases.

## 7. Problem №10: Inverted pendulum

### 7.1. Solution of Korea

#### 7.1.1. Review of solution of Korea

#### **Review of solutions of the problem number №10: Inverted pendulum**

The problem is an interesting problem from both the theoretical and experimental points of view. It opens possibilities to perform a number of experiments at the high-school level using a variety of techniques to provide the oscillations required to stabilise the system. Mathematical solutions of some complexity but based upon concepts already met at high school level should be feasible. Numerous sources of sample theoretical solution to stabilising a single inverted pendulum exist to give guidance but less information is available relating to the situation of an inverted multiple pendulum.

#### **Solution from Korea:**

The solution from Hyeongsu Park of the Korean team concentrates on the situation of a single inverted pendulum and looks at comparing differing methods of achieving the stabilisation required.

The paper references Blitzer's paper "Inverted Pendulum" in the American Journal of Physics, Volume 33, Issue 12, June 1965, pp.1076-1078, but this is not clearly cited within the theory development. Three other references are well cited and used. Given the number of papers on a single inverted pendulum available it is difficult to measure the originality of the solution but the comparison of methods is a nice element and would lead to a useful discussion tool in school physics lessons.

The use of language is confusing at times but the mathematical arguments are well developed and easy to follow. These are supported by clear experimental methods and graphs of the results.

I think it is a good solution of the problem of a single inverted pendulum involving careful research of secondary sources and well conducted experiments. The variety of stabilisation patterns was an interesting finding. It is a little disappointing that the more original problem of an inverted multiple pendulum was not addressed.

**Overall:** A nice report, but with the minor drawback that it addresses only part of the stated problem.

Alan Allinson  
IYPT Australia  
alan@iyptaustralia.org or allinson@bggs.qld.edu.au

## 7. Problem №10: Inverted pendulum

### 7.2. Solution of Ukraine

#### Problem №10: Inverted pendulum

Maxim Anisimov, UPhML KNU,  
Ukrainian Physical and Mathematical Lyceum  
of Kyiv National Taras Shevchenko University, Ukraine

#### The Problem:

*It is possible to stabilize an inverted pendulum It is even possible to stabilize an inverted multiple pendulum /one pendulum the top of the other/. Demonstrate the stabilization and determine on which parameters this depends.*

#### Introduction

Inverted pendulum is an interesting example of the non-linear oscillating system. The main idea of this device is an oscillating point of suspension. In this case, upper position of the pendulum is stable. The motion of the inverted pendulum is a classical example of the motion in the fast-oscillating field.

It was first theoretically investigated by P. L. Kapitza in 1951, so the physical model of the single inverted pendulum is well-known. Kapitza also demonstrated an experimental device to prove his theoretical results.

#### Problem statement.

To build a complete solution, both theoretical and experimental sides of the problem should be considered. Theory proves the possibility of stabilization, and experiment demonstrates it.

#### Physical model.

The main idea of such stabilization is to oscillate the point of suspension vertically with the frequency, lot more than the characteristic one. The motion equation looks as following (general form):

$$\ddot{x} + f(x) = F(x) \cos \Omega t, \quad (1)$$

here  $\Omega \gg \frac{1}{T}$ , where T is the specific period of motion in the system.

The solution X is found as the sum of slow and fast oscillating parts  $x(t)$  and  $\mu\chi(t)$ . After some transformations the equation (1) is rewrote as:

$$\ddot{X} + f(X) + \frac{1}{2} \frac{F(X)}{\Omega^2} \frac{\partial F}{\partial x} \Big|_x = 0$$

We see that additional force appears; it is proportional to the oscillations' amplitude.

Now let's consider the double pendulum, consisting of two point loads on the weightless sticks:

First of all, we write down the coordinates of weights M and m:

$$x_M = L \sin \theta,$$

$$y_M = L \cos \theta + a \cdot \sin \omega t;$$

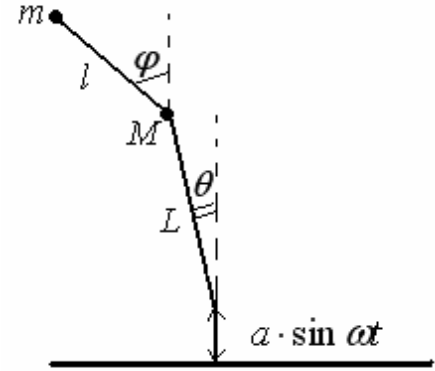
$$x_m = L \sin \theta + l \cdot \sin \varphi,$$

$$y_m = L \cos \theta + l \cdot \cos \varphi + a \cdot \sin \omega t;$$

Now let's evaluate the kinetic ( $T$ ) and potential ( $U$ ) energy of these weights:

$$T_M = \frac{M}{2} (\dot{x}_M^2 + \dot{y}_M^2), \quad T_m = \frac{m}{2} (\dot{x}_m^2 + \dot{y}_m^2);$$

$$U_M = Mgy_M, \quad U_m = mgy_m.$$



Then we write the Lagrange function (the difference  $T-U$ ) for all the system:

$$\begin{aligned} \mathbf{L} = & L^2 \dot{\theta}^2 \left( \frac{M+m}{2} \right) + a^2 \omega^2 \cos^2 \omega t \left( \frac{M+m}{2} \right) - 2a\omega L \cos \omega t \dot{\theta} \sin \theta \left( \frac{M+m}{2} \right) + \\ & + \frac{m}{2} \left( l^2 \dot{\varphi}^2 + 2Ll \cos(\theta - \varphi) \dot{\theta} \dot{\varphi} - 2a\omega l \cos \omega t \sin \varphi \dot{\varphi} \right) - Lg \cos \theta (M+m) - \\ & - ag \sin \omega t (M+m) - mgl \cos \varphi. \end{aligned}$$

Now, using this expression, we can write down the following set of differential equations:

$$\frac{d}{dt} \left( \frac{\partial \mathbf{L}}{\partial \dot{\theta}} \right) = \frac{\partial \mathbf{L}}{\partial \theta}, \quad \frac{d}{dt} \left( \frac{\partial \mathbf{L}}{\partial \dot{\varphi}} \right) = \frac{\partial \mathbf{L}}{\partial \varphi},$$

that describes the motion of double pendulum.

After derivation, simplifying and some transformations we get another system:

$$(M+m) \left[ L\ddot{\theta} + a\omega^2 \sin \omega t \sin \theta - g \sin \theta \right] + ml \left[ \cos(\theta - \varphi) \ddot{\varphi} + \sin(\theta - \varphi) \dot{\varphi}^2 \right] = 0$$

$$l\ddot{\varphi} + (a\omega^2 \sin \omega t - g) \sin \varphi - L \sin(\theta - \varphi) \dot{\theta}^2 + L \cos(\theta - \varphi) \ddot{\theta} = 0.$$

### **Equilibrium condition.**

To solve these equations, we use the same method as for Kapitza pendulum equation. We substitute angles  $\theta$  and  $\varphi$  in the form:  $\theta = \gamma + \alpha$ ,  $\varphi = \delta + \beta$ , where the first terms vary slowly relatively to the second terms. Averaging upon the period of the point of suspension oscillations  $\frac{2\pi}{\omega}$ , one can get the set of 4 equations:

$$(M+m) \left[ L\dot{\gamma} + a\omega^2 \langle \sin \omega t \cdot \alpha \rangle - g\gamma \right] + ml\ddot{\delta} = 0 \quad (2 \text{ a})$$

$$l\ddot{\delta} + a\omega^2 \langle \sin \omega t \cdot \beta \rangle - g\delta + L\dot{\gamma} = 0 \quad (2 \text{ b})$$

$$(M + m)[L\ddot{\alpha} + a\omega^2 \sin \omega t \cdot \gamma - g\alpha] + ml\ddot{\beta} = 0 \quad (2 \text{ c})$$

$$l\ddot{\beta} + a\omega^2 \sin \omega t \cdot \delta - g\beta + L\ddot{\alpha} = 0 \quad (2 \text{ d})$$

In the two last equations one should consider  $\alpha = A \sin \omega t$ ,  $\beta = B \sin \omega t$ , and other variables are constant. Then, finding  $A$  and  $B$  from (2 c) and (2 d), one can get solutions in the form:

$$A = f_1\gamma + f_2\delta,$$

$$B = f_3\gamma + f_4\delta.$$

Then (2 a) and (2 b) look as follows:

$$L\dot{\gamma} + \frac{a\omega^2}{2}(f_1\gamma + f_2\delta) - g\gamma + \mu l\dot{\delta} = 0,$$

$$l\dot{\delta} + \frac{a\omega^2}{2}(f_3\gamma + f_4\delta) - g\delta + L\dot{\gamma} = 0, \mu = \frac{m}{M+m}.$$

We find general solution in the exponential form,  $\gamma \sim \delta \sim e^{\lambda t}$ .

After some transformations we get the characteristic equation for  $\lambda$ :

$$\gamma \delta \left( \lambda^2 L + \frac{a\omega^2}{2} f_1 - g \right) \left( -l\lambda^2 - \frac{a\omega^2}{2} f_4 + g \right) = \delta \gamma \left( -\frac{a\omega^2}{2} f_2 - \mu l \lambda^2 \right) \left( L\lambda^2 + \frac{a\omega^2}{2} f_3 \right)$$

It is biquadrate, and possible roots are  $\pm\lambda_1, \pm\lambda_2$ . For the stable equilibrium they should be purely imaginary, so,  $(\lambda^2)_{1,2} < 0$ . Writing the equation as polynomial of  $\lambda$ , one can get:

$$\begin{aligned} \lambda^4 (Ll - \mu lL) + \lambda^2 \left( \frac{La\omega^2 f_4}{2} - Lg + \frac{a\omega^2 fl}{2} - gl - \frac{a\omega^2 f_2 L}{2} - \frac{\mu la\omega^2 f_3}{2} \right) \\ + \frac{a^2 \omega^4 fl f_4}{4} - \frac{a\omega^2 fl g}{2} - \frac{ga\omega^2 f_4}{2} + g^2 - \frac{a^2 \omega^4 f_2 f_3}{4} = 0 \end{aligned}$$

or

$$A\lambda^4 + B\lambda^2 + C = 0.$$

We designate coefficients near  $\lambda$  by A,B,C, where A>0. According to the Wiet theorem, to find the equilibrium, the following conditions should be fulfilled:

$$B > 0$$

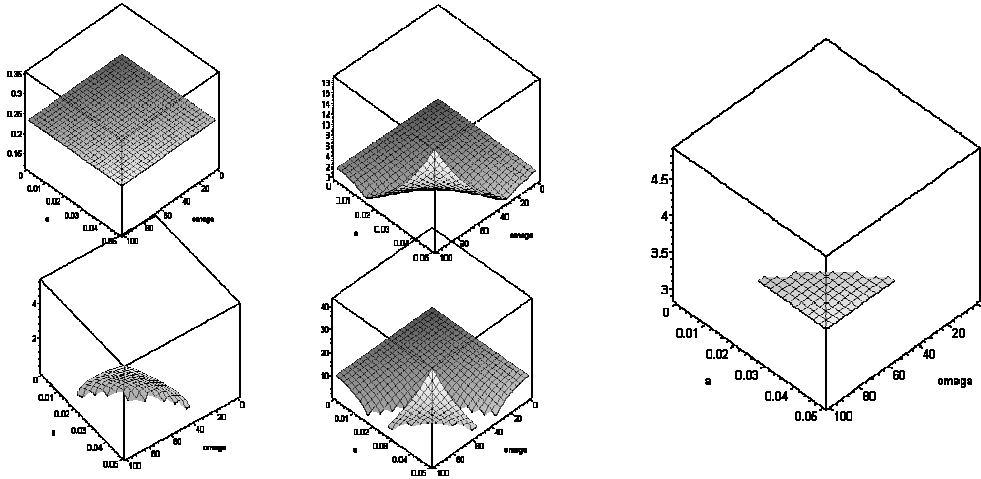
$$C > 0$$

$$D = B^2 - 4AC > 0$$

It's difficult to solve these inequations manually, but with the help of computer it's possible to get numerical dependences of A,B,C,D on the frequency and amplitude.

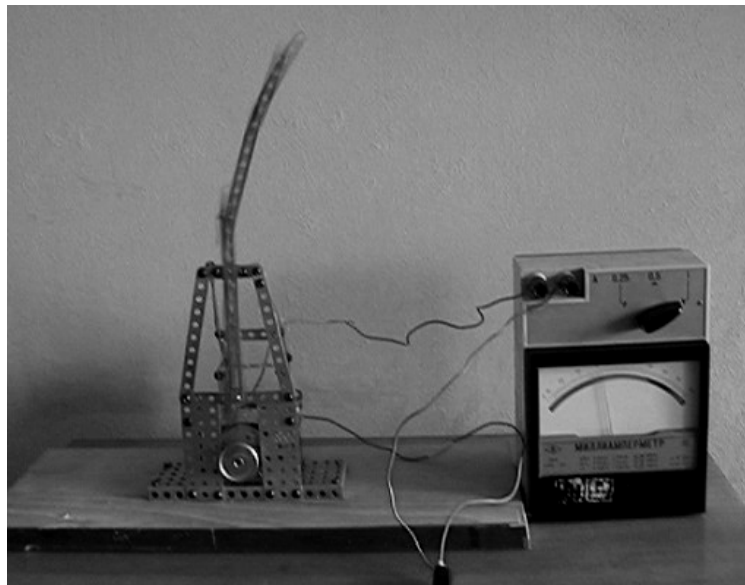
*Graphs showing dependence upon amplitude and frequency,*

*built with Maple 8 (Constants: M = 0.1; m = 0.01; L = 0.3; l = 0.2).*



### *Experiment.*

To demonstrate the real stabilization, our team constructed an experimental device. Its photo is shown below:



### *Conclusions.*

To solve the problem theoretically, known physical model of a single inverted pendulum was considered. It was used as a basic one to build the theory of double pendulum. Resulting solution determines the possibility of stabilization, depending on initial conditions, which are inputted numerically.

The presented problem solution demonstrates an example of the physical modelling of non-linear oscillating systems.

## 8 Problem № 11: Singing tube

### 8.1. Solution of Australia

#### Problem №11: Singing tube

Kathryn Zealand, Brisbane Girls Grammar School, 47 Verney Rd. West, Graceville, Brisbane, QLD 4075, Australia, s106863@bggs.qld.edu.au

#### The Problem:

*It is possible to stabilize an inverted pendulum It is even possible to stabilize an inverted multiple pendulum /one pendulum the top of the other/. Demonstrate the stabilization and determine on which parameters this depends.*

#### 1. Abstract

The Rijke or Singing Tube is a vertical tube with metal gauze inserted in the lower half. After heating the gauze, a loud sound is produced. By investigating many aspects of the Singing Tube phenomenon, it was discovered that during a compression, cool air is drawn in and heated, this causes its pressure to change, augmenting the pressure maximum. This action creates and sustains the acoustic wave, however when determining the optimum gauze position, the two factors of consideration disagree. The Rayleigh Criterion and Rayleigh Index provide a more precise model of the relationship between gauze position and sound intensity. Expressions for heat transferred from the gauze, and where this heat was lost to provide insight into the mechanisms which determine how long the singing can be sustained, and thus what variables to experimentally investigate, these included tube length, diameter, material, shape and the gauze's heating time.

#### 2. Interpretation

We were asked to investigate the 'singing' produced by an open tube over a flame. We defined 'singing' as a loud sound with definite frequencies, and minimal variation in sound intensity. We tried producing a sound with just a tube over a flame; however, we did not count this quiet and raspy sound as 'singing'. Research suggested that adding a piece of gauze inside the pipe would enhance the noise to a louder and measurable 'singing' tone. Therefore, we concentrated on this interpretation of a singing tube (also called the Rijke<sup>8</sup> tube).

#### 3. Basic Theory

There were 2 phases of heating, in the initial heating phase, the Bunsen heats the gauze, yet no sound is produced. After removing the heat source, the tube 'sang' for a period of time before stopping. To understand how this creates sound, some basic theory is needed.

##### 3.1. Waves

Sound or Acoustic waves are longitudinal, meaning that the particles vibrate in the direction of the wave's propagation. A sound wave is made of compressions (areas of high pressure) and rarefactions (areas of low pressure). Particle displacement and pressure variations can be modelled by the sinusoidal functions [1]:

---

<sup>8</sup> P.L. Rijke was a professor of physics at the University of Leyden in the Netherlands when, in 1859, he discovered this phenomenon

$$s(x, t) = s_m \cos(kx - \omega t)$$

$$\Delta p(x, t) = \Delta p_m \sin(kx - \omega t)$$

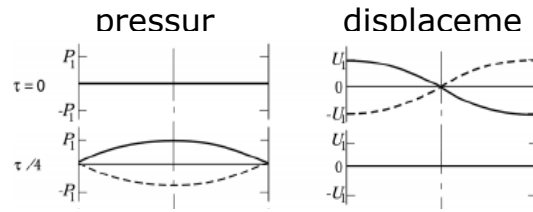


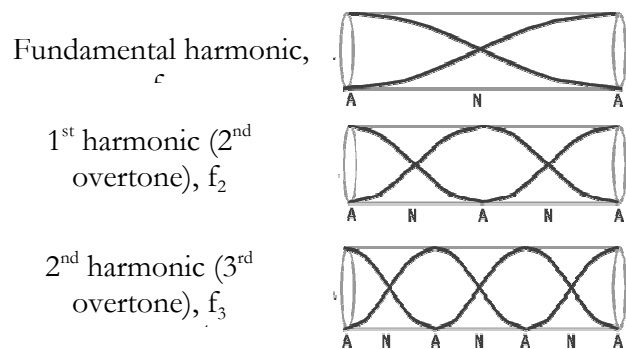
Figure 11 Pressure and Displacement functions are out of phase

Where  $\omega$  is the angular velocity,  $p$  is the pressure,  $k$  is the wave number,  $s_m$  is the displacement amplitude and  $p_m$  is the pressure amplitude. The pressure and displacement functions are out of phase.

Hot air is less dense than cool air, so will rise. An initial compression is caused by the rising hot air, as the static air above it will ‘bunch up’ causing a compression. This hot moving air will also cause a pressure difference between the inside of the tube and the ambient outside pressure, so a pressure barrier at the end is formed. Some of the initial compression will then reflect of this barrier back down the tube. The reflected compression will constructively or destructively interfere with the rising hot air forming a standing wave.

### 3.2. Standing Waves and Resonance

The standing wave is cause by the interference of the reflected wave on itself. A standing wave consists of nodes (areas of least particle and velocity displacement) and antinodes (areas of maximum particle and velocity displacement). The standing wave causes us to hear a continual tone. Resonance is caused when the standing wave is continually reinforced, the amplitude is increased creating a very loud sound, the air column in the pipe is said to resonate.



### 3.3. Harmonic frequencies

For the tube to resonate, the tube length must be a multiple of half wavelength of the standing wave, we can express this as  $n\lambda=2L$ , where  $\lambda$  is the wavelength, and  $L$  is the tube length. The first harmonic is called the fundamental harmonic ( $f_0$ ) and only has one nodal point in the tube. Higher harmonics are multiples of the fundamental (see figure 2).

From the wave equation,  $v=f\lambda$ , where  $v$  is the velocity of sound, and the relationship above, we can derive a formula for the frequency [2].

$$v = f\lambda = f \frac{2L}{n} \quad n\lambda = 2L \quad f = \frac{nv}{2L}$$

However, the air particles also vibrate with a slight sideways motion, and beyond the end of the tube. This results in a necessary ‘end correction’ [3], where  $d$  is the diameter of the tube.

$$f = \frac{nv}{2L + 0.8d}$$

For the fundamental frequency ( $n=1$ ), and at a temperature of  $34^{\circ}\text{C}$  (where  $v$ , the speed of sound is  $351\text{ms}^{-1}$ ), the frequency becomes:

$$f = 175.5 \left( \frac{1}{L + 0.4d} \right)$$

#### 4. Sustaining the acoustic wave

Some of the wave and thus energy escapes and is emitted at the end of the tube. Therefore heat energy must be added to sustain the oscillations. There must also be a continuous air flow; we demonstrated this by turning the tube to horizontal, which removed the thermal convection. As predicted, the tube did not sing.

##### 4.1. Velocity and Pressure Fluctuations

The flow past the gauze is a combination of two motions. There is a uniform upward velocity, caused by the rising hot air, and a varying velocity,  $u'$  caused by the sound wave (oscillatory particle vibration velocity).

There is an ambient or mean pressure, as well as the varying pressure,  $p'$  caused by the compressions and rarefactions of the acoustic wave.

##### 4.2. Amplifying the wave

For half the cycle, the varying and uniform velocities are in the same direction, which is when the particles around the gauze are vibrating upwards, in the same direction as the thermal convections. Therefore, air will be drawn up into the tube until pressure reaches a maximum. Most of this air will already be warm (having been expelled from the hot tube during the last cycle). However just before the pressure reaches a maximum, some cool air is drawn in, this is because the uniform thermal convection pushed some of the warm air out of the top of the tube last cycle. This cool air is quickly heated by the hot gauze, so there is a large heat transfer. This causes the (previously cool) air's pressure to increase, adding to the pressure maximum. Therefore, although energy is being lost at the top of the tube, every cycle a small part of the gauze's heat energy is used to increase the pressure maximum, thus amplifying the wave.

##### 4.3. Optimum gauze position

Since the singing is caused by cool air increase in pressure, there two things which must be considered when determining the optimum gauze position. First, the placement of the gauze should be such that the amount of cool air heated is optimised. As it is the combination of varying and uniform particle velocity that determines how much cool air gets heated, this would suggest that the gauze should be placed where the varying velocity is at a maximum, at the anti-node, for the fundamental frequency, the anti-node is at the end of the tube.

The second aspect to consider is where the cool air's pressure increase will have most impact. The pressure increase reinforces the varying acoustic pressure, but at an anti-node, the varying pressure is zero, so placing the cool air's pressure increase would have no effect. The

varying pressure is at a maximum at a node, so according to this, the gauze should be placed at a node, which is at the middle of the tube for the fundamental frequencies.

These aspects clearly disagree, so all this tells us is that the optimum position is a compromise, somewhere between the end and middle of the tube. The Rayleigh Criterion is a mathematical description of the interaction between pressure and velocity fluctuations and allows for more precise optimisation of gauze placement.

## 5. The Rayleigh Criterion

As energy escapes at the top end of the tube, to sustain the acoustic wave, heat energy must be added at certain points, according to the Rayleigh Criterion [5]; “If heat be given to the air at the moment of greatest condensation, the vibration is encouraged”. This means that most heat must be added in a compression. Please see section V of the Onera short lecture course of Combustion instabilities in liquid rocket engines [6] for a mathematical proof and derivation of the Rayleigh Criterion.

### 5.1. Velocity and Heat Transfer

When there is a large heat transfer, many particles get heated and thus, many rise, this creates a large varying velocity. So the heat transfer,  $Q'$  creates the varying velocity,  $u'$ .

As mentioned previously, when cool air is drawn in, heat is transferred easily so the heat transfer,  $Q'$  is large. When the varying velocity,  $u'$  is down and against the upward flow, there is little airflow, less cool air is drawn in, and the gauze is surrounded by warm air. Therefore there is less heat transfer,  $Q'$  is small.

So  $Q'$  varies with  $u'$ , and there may be a time lag (as it is a cause and effect, rather than simultaneously). This can be expressed by:  $Q' \propto u'$ . Where  $\tau$  is the time lag. In summary, the heat transfer creates the varying velocity, and it is sustained by the varying velocity, so once the cycle is initiated, the waves are sustained.

### 5.2. Rayleigh Criterion Integral

The Rayleigh Criterion can be expressed as “If  $p' > 0$  and  $Q' > 0$  or  $p' < 0$  and  $Q' < 0$ , the wave is sustained” where  $p'$  is the acoustic pressure, and  $Q'$  is the heat transfer. A convenient way to express this statement is in the following integral, where  $T$  is the period of the wave, and  $R$  is the Rayleigh index [7]:

$$R = \frac{1}{T} \int p' Q' dt$$

The Rayleigh Criterion can now simply be expressed as if  $R > 0$  the wave is amplified. Sound intensity will be greatest when  $R$  is maximised.

### 5.3. Optimum gauze position

The optimum gauze position (for sound intensity) will occur where the Rayleigh Index,  $R$ , is maximised. It was seen in section 5.1, that the heat transfer is proportional to the varying velocity,  $Q' \propto u'$  so  $R$  is proportional to the product of acoustic pressure and velocity.

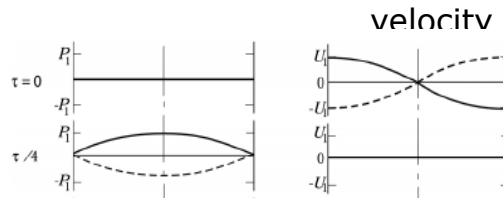
$$R = \frac{1}{T} \int p' Q' dt \Leftrightarrow R \propto \frac{1}{T} \int p' u' dt$$

$\therefore R \propto p' u'$

Now we need to maximise  $p' u'$ . It was explained in section 3.1, that the acoustic pressure and velocity are sinusoidal:

$$u'(x,t) = u'_m \cos(kx - \omega t)$$

$$p'(x,t) = p_m \sin(kx - \omega t)$$



Since we are only concerned with proportionality, and  $u_m$  and  $p_m$  are constants (maximum amplitudes), they can be neglected:

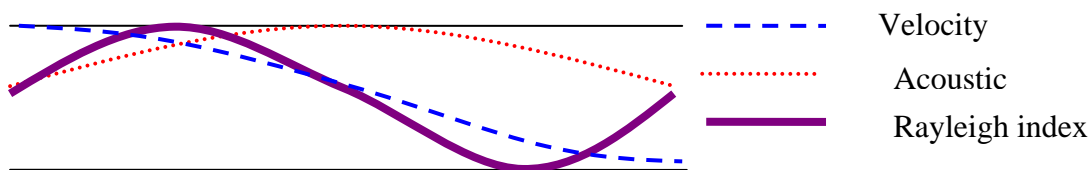
$$R \propto \cos(kx - \omega t) \sin(kx - \omega t)$$

Here we can substitute in the trigonometric identity,  $2 \sin x \cos x = \sin 2x$ :

$$R \propto \frac{1}{2} \sin 2(kx - \omega t)$$

$$R \propto \sin 2(kx - \omega t)$$

This function has a similar shape to the function for acoustic pressure, but it has half the period, therefore, R will be at a maximum halfway between the end of the tube and the node in the centre of the tube, where the pressure has a maximum:



N.B. waveforms are for comparative purposes only; the amplitude of the Rayleigh index would be different due to constants of proportionality

Figure 4 Diagram showing that the Rayleigh index is proportional to the product of velocity and pressure, and is at a maximum 25% up the tube, thus this is the optimum position for the gauze

So the optimum gauze position is where R is at a maximum, which is 25% up the tube, and the sound intensity should follow a similar sinusoidal curve to the Rayleigh index as the gauze is moved along the tube. This supports the qualitative explanation presented in section 4.4.

#### 5.4. Gauze in upper half of tube

However, by this logic, a sound should be created when the gauze is 75% up, as this is also halfway between the fundamental node and anti-node, however, the cool air is drawn towards the centre just before the pressure maximum, and is pushed up past the centre after the pressure maximum. When the gauze is in the top half, the



Figure 12 Using a vacuum cleaner to reverse the air flow, changing the optimum gauze position

cool air is heated just before the pressure minimum, so the increase in the cool air's pressure cancels the acoustic decrease in pressure, thus diminishing the sound.

We proved this by reversing the direction of the thermal convections with a vacuum cleaner. This pushed cool air in from the top rather than the bottom. When using an artificial air flow, a sound was created with gauze in the top half.

## 6. Heat Transfer

It has been demonstrated that the gauze will transfer little heat in a rarefaction, and lots in a compression, but how much heat is transferred, and what effect will this have on the singing time? Expressions for the amount of heat transfer will be derived in the following sections.

### 6.1. Heat Transfer Expressions

Let us first examine where the heat from the gauze is lost to heating the air to provide the uniform thermal convection, sustaining the acoustic wave (heat transferred to cool air, discussed in section 7), and losses, which will be predominantly through conduction to the tube walls. The heat absorbed by the gauze through heating must transformed to the energy forms listed above, as energy is conserved, these must be equal.

This can be expressed in a differential equation as;

$$\frac{dQ_{gauze}}{dt} = \frac{dQ_{convection}}{dt} + \frac{dQ_{emitted\ wave}}{dt} + \frac{dQ_{losses}}{dt}$$

Where  $dQ/dt$  is the rate of heat transferred (measured in Joules per second). The standard equation for heat transfer to the gauze during heating is [2]:

$$\frac{dQ_{absorbed\ by\ gauze}}{dt} = c_g m_g \frac{dT_{gauze}}{dt}$$

Where  $c_g$  is the specific heat capacity of the gauze,

$m_g$  is the mass of the gauze, and  $dT/dt$  is the change in temperature of the gauze. The heat lost through convection to the air can also be modelled by the standard heat transfer equation [2]:

$$\frac{dQ_{lost\ through\ convection}}{dt} = c_{air} m_{air} \frac{dT_{air}}{dt}$$

Where  $c_{air}$  is the specific heat capacity of air,  $m_{air}$

is the mass of air, and  $dT/dt$  is the change in temperature of the air, after passing the gauze. The average rate at which kinetic energy,  $E_k$  of a sound wave escapes can be expressed as: [1]

$$\frac{dQ_{emitted\ wave}}{dt} = \frac{dE_k}{dt} = \frac{1}{16} \rho A v \omega^2 s_m^2$$

Where  $\rho$  is the density of air,  $A$  is the cross-

sectional area of the tube,  $v$  is the velocity of the wave,  $\omega$  is the angular velocity, and  $s_m$  is the displacement amplitude. Most of the losses will be thermal conduction to the tube walls, this can be modelled as follows:

$$\frac{dQ_{tube}}{dt} = kA(T_{hot} - T_{cold}) \Leftrightarrow \frac{dQ_{tube}}{dt} = kA \frac{dT_{tube}}{dt}$$

Where k is the thermal conductivity co-efficient. These components can now be combined, so the original equation:

$$\frac{dQ_{gauze}}{dt} = \frac{dQ_{convection}}{dt} + \frac{dQ_{emitted\ wave}}{dt} + \frac{dQ_{losses}}{dt} \quad \text{Becomes:}$$

$$m_g c_g \frac{dT_{gauze}}{dt} = m_{air} c_{air} \frac{dT_{air}}{dt} + \frac{1}{16} \rho A v \omega^2 s_m^2 + kA \frac{dT_{tube}}{dt}$$

6.2. What can this expression tell us?

This expression reveals the limiting factor which affects how much heat must be given to the gauze for singing to occur, and how long the tube will sing for. The tube will start singing when:

$$\frac{dT_{gauze}}{dt} \geq \frac{1}{m_g c_g} \left( m_{air} c_{air} \frac{dT_{air}}{dt} + \frac{1}{16} \rho A v \omega^2 s_m^2 + kA \frac{dT_{tube}}{dt} \right)$$

To keep singing, the gauze must have enough heat or a large enough temperature gradient to provide constant heat to the air convections and losses to the tube. So the tube will stop singing when:

$$\frac{dT_{gauze}}{dt} \leq \frac{1}{m_g c_g} \left( m_{air} c_{air} \frac{dT_{air}}{dt} + \frac{1}{16} \rho A v \omega^2 s_m^2 + kA \frac{dT_{tube}}{dt} \right)$$

Therefore, this expression reveals many factors and variables which affect the onset and discontinue of the singing. The type of gauze will have an effect since the expression starts,  $\frac{1}{m_g c_g}$ , and both the mass and specific heat capacity are properties of the gauze, since it is the

inverse of mass, the tube should sing for earlier and for longer when a heavier gauze is used, since a heavier gauze could absorb more heat. The atmospheric conditions will also affect the singing, since at different temperatures and humidities, the specific heat capacity of air changes. Also, if the air starts of warmer, then the change in temperature as it passes the gauze ( $dT_{air}/dt$ ) would be less. This is why all the trails for an experiment were conducted on the same day, or when the temperature is similar (within 3 degrees).

The cross sectional area, A, which is directly proportional to the diameter, appears in all three terms on the left had side of the heat transfer expression ( $m_{air} = Avpt$ )

and so that is why the cross sectional area was a controlled variable in experiments, and tube diameter was chosen to be investigated as an independent variable.  $s_m$



Figure 13 vacuum cleaner used to replace the thermal convection, the tube sings in a horizontal

in 3<sup>rd</sup> term is the displacement amplitude, it describes how far the particles vibrate and thus determines sound intensity. This is why either sound intensity or singing time were measured, because they effect each other.

In the very last term,  $kA \frac{dT_{tube}}{dt}$ , k is the thermal conductivity co-efficient, which is a property of the material, this highlighted the importance that the tube material has, which is why the material was investigated as an independent variable, and controlled in all other experiments.

## 7. Stopping the singing

There are three methods of stopping the tube from singing; hold the tube horizontally, place heat source under tube, and let the gauze cool.

When the tube is held horizontally, there is no thermal convection, so no cool air brought in contact with the gauze, so the wave cannot be amplified (we demonstrated that it was the lack of thermal convection preventing amplification by using a vacuum clean to produce artificial convections). When the Bunsen burner or another heat source is under the tube, the air passing the gauze has already been heated, so with no heat transfer possible, there is no pressure increase to sustain the acoustic wave. As the gauze losses its heat energy to the passing air, it will gradually cool, until it is no longer able to supply enough energy to facilitate a pressure increase, and sustain the wave.

## 8. Cold Gauze

The change in temperature between the gauze and the air causes the phenomenon; therefore, a similar sound can be produced with a gauze which is cooler than the surrounding air. A weak sound was produced when cold gauze (from freezer is sufficient in the Brisbane summer) was inserted 25% up the tube. The cold gauze causes a downwards convection current, so warmer air is drawn in at top just before the pressure maximum, and reaches the gauze in the bottom half just before the pressure minimum, the warm air is rapidly cooled by the gauze, its pressure decreases, enforcing the pressure minimum.

## 9. Our Investigations

### 9.0. General Procedure

The 1mm steel gauze was inserted ¼ of the way up each tube. The Bunsen burner was slid under the tube and 10 seconds later, the Bunsen burner was removed and another person recorded the singing with the microphone. This was repeated for all the tubes, five times then averaged.

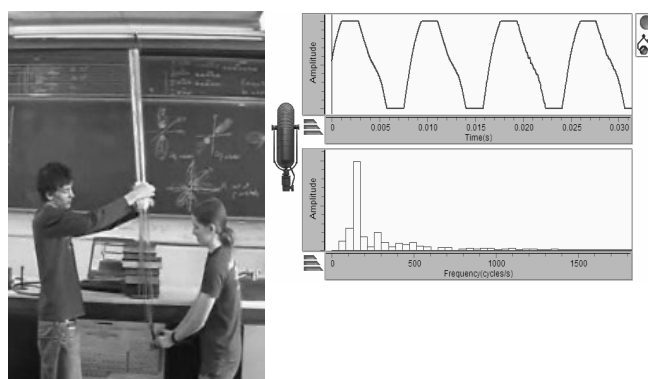


Figure 14 Sample datum collected and demonstration

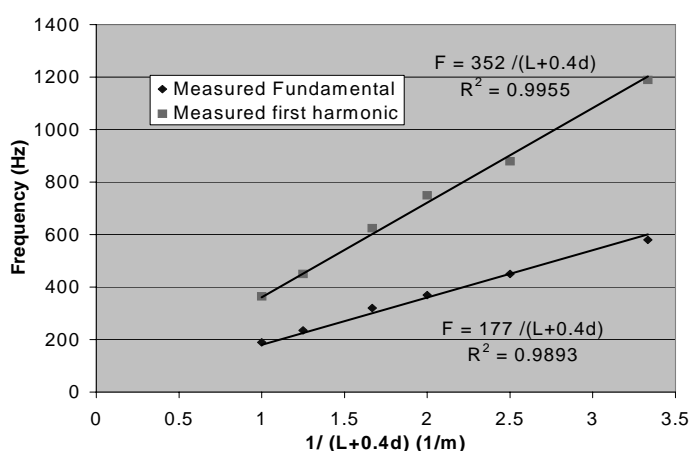
## 9.1. Tube Length

### 9.1.1. Hypothesis

As the tube length increases, the wavelength of the sound will increase, and therefore its frequency will decrease. The frequency and tube length should have the following relationship:  $f = 175.5 \left( \frac{1}{L + 0.4d} \right)$ . As the tube diameter was constant, the graph of frequency

vs.  $\frac{1}{L + 0.4d}$  should be linear.

### 9.1.2. Results



There was an audible difference in pitch between the ‘singing’ from the larger and smaller tubes, this is evidence that the frequency was changing. The longer tubes produced a weaker tone.

Figure 4 Graph of results from Tube Length experiment, linear relationship

### 9.1.3. Discussions

We derived in section 4.3 that the fundamental frequency (at 34°C) was given by:  $f = 175.5 \left( \frac{1}{L + 0.4d} \right)$  So in the above graph, a linear relationship predicted, with a gradient of 175.5. In the experimental results, the linear relationship is reasonable since the datum points are scattered on both sides of the line, the  $R^2$  value is 0.9893, and the uncertainties are small. The measured gradient was  $177 \pm 4$ . Therefore, the Harmonic equations derived in section 4 are accurate (within the uncertainty) and our hypothesis was supported. We have also consolidated the knowledge on which these equations were derived.

### 9.1.4. Conclusions and Reflections

In section 9.1.3.1. it was observed that the sound volume and therefore intensity decreased as the tube length increased, this was unexpected, and upon further qualitative experiments, when heated for a longer period of time, the longer tubes ‘sung’ with more intensity than the shorter ones. One possible explanation for this discrepancy is that in longer tubes, the gauze is further from the Bunsen burner flame, so more of the flames heat may have been used to heat the longer air column and tube wall in the longer tubes than in the short tubes. Hence, an improvement to the procedure would be to measure the temperature of the gauze, and

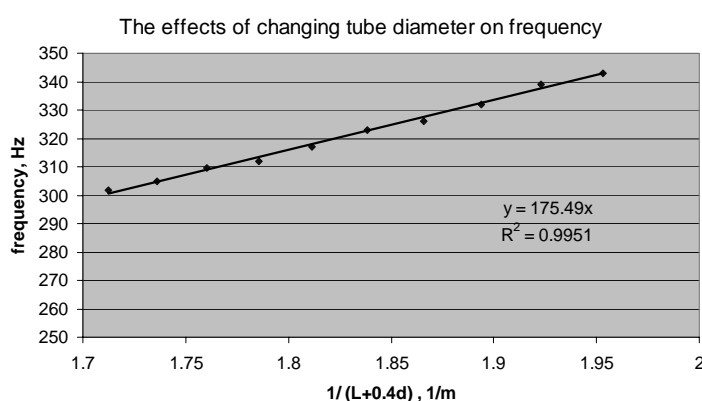
stop heating once a certain temperature had been attained, rather than heating for a specific duration of time.

## 9.2. Tube Diameter

### 9.2.1. Hypothesis

As the tube diameter increases, the frequency will decrease. The relationship should be  $f = 175.5 \left( \frac{1}{L+0.4d} \right)$ . In this experiment, the tube length, L was constant, so the graph of frequency vs.  $\frac{1}{L+0.4d}$  should be linear, with a gradient of 175.5.

### 9.2.2. Results



For tubes bigger than 20cm in diameter, it became increasingly difficult to produce a sound. The larger diameter tubes had a larger sound intensity until they stopped producing a sound. There was very little audible variation in pitch, since the frequency only varied ~10%.

Figure 6 Graphed results from Tube Diameter experiment, linear relationship

### 9.2.3. Discussions

We derived in section 4.3 that the fundamental frequency (at 34°C) was given by:

$f = 175.5 \left( \frac{1}{L+0.4d} \right)$  Experimentally, there was a linear relationship between the frequency

and  $1/(L+0.4d)$ . Since the points are scattered both sides of the line, with an  $R^2$  value of 0.9952, this relationship is reasonable. In the above graph, the predicted gradient was 175.5, and the measured gradient was  $174 \pm 5$ . Therefore, (within the uncertainties), it has again been shown that these Harmonic equations are accurate. We have also supported our hypothesis, that as the tube diameter increases, the sideways vibration of the particles and therefore the tube's end correction increases, thus frequency will slightly decrease. However, it was observed in section 5.2.3.1 that this effect was less noticeable than it was when changing the tube length in experiment 5.1. This is because in our derived equations, tube diameter is multiplied by 0.4, so is decreased, and the diameter of all the tubes was less than their length, thus changing the diameter of the singing tube had less of an effect than changing the length. The increase in sound intensity with increasing tube diameter is due to a larger air flow since there is more hot gauze available to heat the air and cause the thermal convections.

### 9.2.4. Conclusions and Reflections

In section 5.2.3.1, it was observed that it became difficult to produce a sound when the tube diameter was greater than 0.20m, and the sound intensity decreased. A possible explanation for this is that with a wide tube, the barrier of pressure difference necessary for the travelling wave to reflect and cause a standing wave becomes unstable and weak, due to a less defined 'end' of the tube. This would cause only some or none of the wave to be reflected, producing a weaker standing wave. One possible method of testing this would be to use a very sensitive pressure probe, so detect the strength and location of the barrier, such a sensitive instrument was not available for our use.

## 9.3. Tube Shape:

### 9.3.1. Hypothesis

Since it is the column of air that resonates, not the tube its self, changing the horizontal shape of the tube should have no effect, as long as the tube still contains a region of air.

### 9.3.2. Results

Shape Approximation						
% change in diameter	200	400	50	25	0 (centre =200%)	0
observation	Weak sound	No sound	Normal sound	No sound	Gauze wouldn't stay in, No sound	Slightly weaker sound
Frequency	221	-	226	-	-	213

**Table 4 Frequency and observation results from Tube Shape experiment**

### 9.3.3. Discussion

There did not appear to be any clear trend in changing frequency (all values were within the 23Hz margin of error). In addition, our hypothesis was supported in the fact that the frequency is independent on the shape (this is because the tubes purpose is to channel the rising hot air, and provide boundaries for the air column that resonates, neither of these properties are affected by slight changes in tube shape.)

### 9.3.4. Conclusions and Reflections

Tube shape has little effect on frequency.

It was observed in section 5.3.3.1 that for some shapes, the sound was weak or non-existent, which contradicts the hypothesis that shape has no affect. A possible explanation is that it is not the shape of the tube that is inhibiting sound production, but rather the diameter at either end. As experienced in section 9.2.3.1, if the diameter at the top or bottom of the tube is too great, no definite barrier of pressure exists, so the standing wave cannot be created. A possible further experiment would involve using tubes of the same proportion, or same percent increase in diameter, but are smaller, as this would determine if a breakdown in the pressure barrier was responsible for the weaker sound. The curved tube may have produced a

weaker sound because the Bunsen's heat was not directly under the gauze (it was under the end of the tube), so the gauze may not have been heated as effectively.

#### 9.4. Tube Shape:

##### 9.4.1. Hypothesis

Since it is the column of air that resonates, not the tube its self, changing the vertical cross section of the tube should have no effect on the frequency and sound intensity, as long as the tube still contains a region of air.

##### 9.4.2. Results

	Circular	Square	Triangle
Frequency (Hz)	235	235	237
Observation	Loudest sound	Weak sound	Weak sound

**Table 5 Frequency and observational results from the Tube Shape (horizontal) experiment**

##### 9.4.3. Discussion

Since sound is a longitudinal wave, and it is the air not the tube that resonates, there was no noticeable effect on frequency (within the 10Hz uncertainty), supporting the hypothesis. The observation of the sound being strongest with the circular tube was unexpected, and difficult to explain, our best inference is that there is more air flow in circular tube because the triangular and square tubes had corners, and a larger internal surface area. This may cause a larger boundary layer, so the air flows slower in the corners and the gauze in the corner areas doesn't heat as well, so the useable area in the square and triangle is effectively reduced to that of a smaller circle (see figure 4). This would account for the decrease in sound intensity.

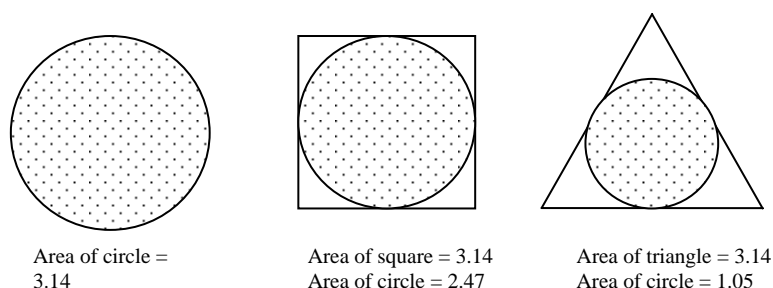


**Figure 7 Although all tubes had the same area, this diagram shows that since air got caught in the corners, the shaded usable area likely decreased.**

### 9.4.4. Conclusions and Reflections

Tube shape had little effect.

An interesting further experiment would involve electrically heating the gauze, to ensure even heating, and having an artificial airflow through the tube, this would help determine if the reasons behind the observed changes in sound intensity.

## 9.5. Tube Material

### 9.5.1. Hypothesis

We saw in section 6 that if the change in temperature of the gauze becomes less than that required to heat the convecting air, the tube will stop singing, this was explained thus: when

$$\frac{dT_{gauze}}{dt} \leq \frac{1}{m_g c_g} \left( m_{air} c_{air} \frac{dT_{air}}{dt} + \frac{1}{16} \rho A v \omega^2 s_m^2 + kA \frac{dT_{tube}}{dt} \right)$$

The tube stops singing. The  $k$  in the last term is the thermal conductivity of the tube. So from this equation we can see that as the thermal conductivity of the material decreases, the tube will sing for longer, as the gauze needs a lower temperature to sustain the wave. When the thermal conductivity of the tube material increases, the gauze needs more heat, and so will not be able to sustain the singing for as long. As sound is a longitudinal wave, the tube acts only as the boundary for the air column inside which vibrates, therefore the frequency should be unaffected by the tube material.

### 9.5.3. Results

Material	iron	steel	aluminium	PVC	wood	Glass	Paper	Plastic	cardboard
Thermal conductivity	79.5	50.2	205	0.19	0.1	0.8	0.05	0.02	0.07
frequency	218	219	215	223	223	223	-	-	223.5
Singing time	26	27	24.3	39.1	39.5	37	-	-	40

Table 6 Frequency and Singing time results for materials of different thermal conductivities

The paper and thin plastic tubes did not sing because they combusted.

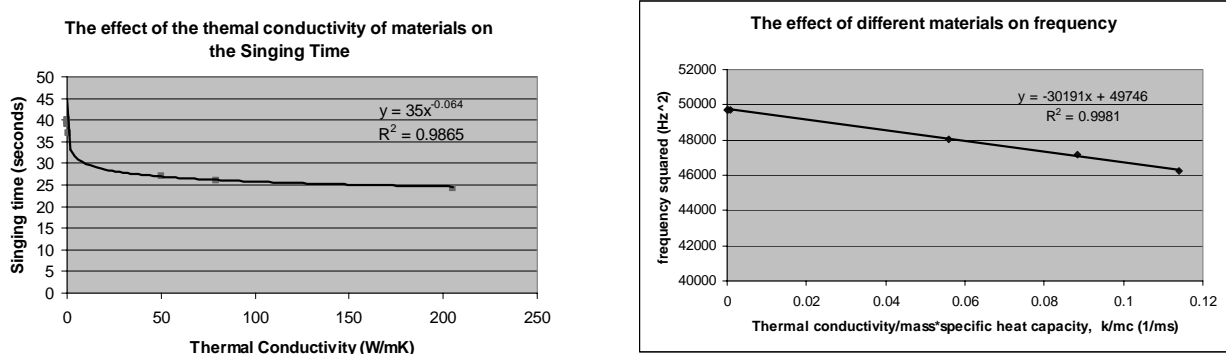


Figure 9 The effect of thermal conductivity of the tube on the Singing time and frequency

#### 9.5.4. Discussion

The hypothesis stated that as the thermal conductivity increased, the tube should sing for less time, since more of the gauze's heat was conducted away to the tube. This was supported experimentally and an exponential relationship was found. However, the hypothesis stated that there should be no effect on frequency, however this is not what we found experimentally; there was variation in frequency for the different materials. Therefore, after brainstorming the differences in the materials, and what could cause the frequency to change, the relationship was realised. Some materials conduct heat away from the gauze and air more than others. Tubes with a high thermal conductivity will conduct heat away from the gauze easily, so the gauze is cooler and will not sing as long as it will in tubes with a low thermal conductivity. Recall from section 4.3. the equation for frequency:

$$f = \frac{v}{2L + 0.8d} \xleftarrow{\text{for same sized tubes, L and d are constant}} f \propto v$$

As long as the tube length and diameter are kept constant, the frequency is directly proportional to the velocity of sound. However, the speed of sound is not constant, it depends upon the temperature.

$$v = \sqrt{\gamma RT} \xleftarrow{\text{R and } \gamma \text{ are constants}} v \propto \sqrt{T} \quad [4]$$

So now it is clear that frequency has a squarely relationship with temperature:  $f \propto \sqrt{T} \Leftrightarrow f^2 \propto T$  However, we do not know how the different materials change the temperature in the tube. Recall the equations regarding temperature and heat from section 6, the information concerning their thermal conductivity,  $k$ , and specific heat capacity,  $c$  is available. Thermal conductivity is a measure the rate at which heat is transferred per unit area. Since all the tubes had the same dimensions, Heat lost is proportional to the thermal conductivity,  $Q \propto k$ .

Heat lost can also be expressed in terms of the mass and specific heat capacity of the tubes,  $Q = mcT$ . Therefore, it means that:

$$f^2 \propto T$$

$$Q = mcT \propto k \Leftrightarrow T \propto \frac{k}{mc}$$

So this predicts that a  $\therefore f^2 \propto \frac{k}{mc}$  graph of  $f^2$  vs.  $k/mc$  should be linear. Experimentally a linear relationship was found. This relationship is reasonable since the  $R^2$  value is 0.9981. The relationship had a gradient  $-30000 \pm 1200$ , and intercept of  $50000 \pm 4000 \text{Hz}^2$ . This means that if the tube were a perfect insulator ( $k=0$ ) then the frequency would be  $223 \text{Hz} = \sqrt{50000}$

#### 9.5.5. Conclusions and Reflections

Frequency and the thermal conductivity of the tube have the following relationship:

$f^2 = -30000 \frac{k}{mc} + 50000$ . It was felt that this experiment could be improved by having materials with a wider range of thermal conductivity values, as the PVC, wood, glass and cardboard tubes all had similar values. Although the hypothesis was proved incorrect, more interesting discoveries were made as a result.

## 9.6. Gauze Position

### 9.6.1. Hypothesis

It was discovered in section 5.3. that the Rayleigh Index and therefore the sound intensity follow a sinusoidal function with respect to the position of the gauze in the tube. This sine curve has a period of the length of the tube (100%), and a maximum at 25%. The graph of sound intensity vs. the sine of the product of 3.6 and gauze position should be linear. (3.6 alters the normal period of the sine function ( $360^\circ$ ) to the length of the tube, 100 (%).  $3.6 = 360/100$ )

### 9.6.2. Results

The tube did not sound at all when the gauze was in the upper half. The computer program recorded background noise, so although seven was the lowest sound intensity recorded, the tube did not contribute to this, and was silent at the time.

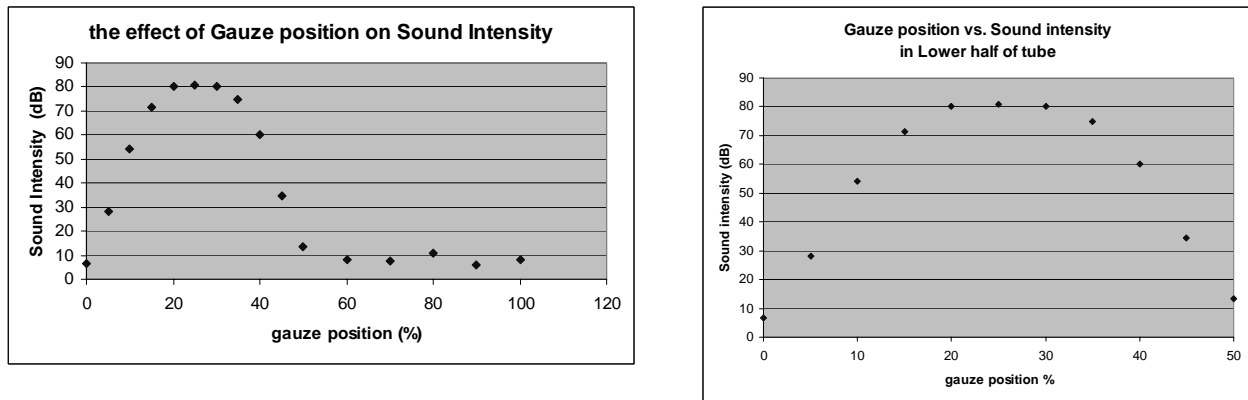


Figure 10 Graphed results for sound intensity from the Gauze Position experiments

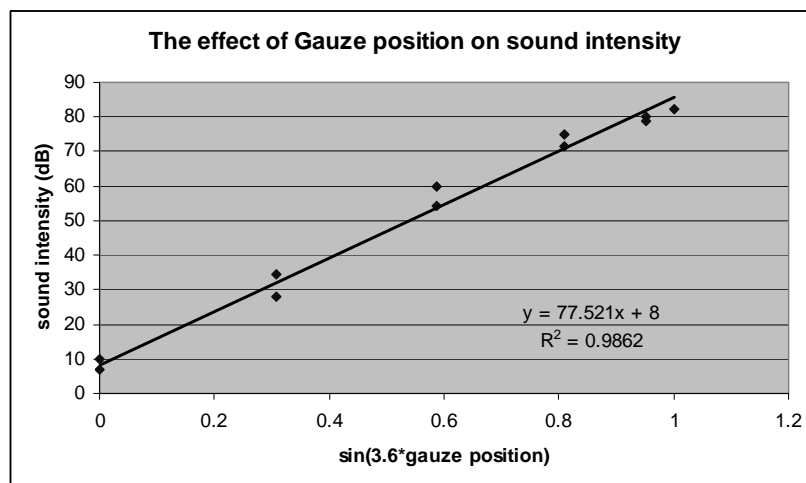


Figure 8 Linear relationship of Gauze position results

#### 9.6.4. Discussion

As predicted, sound intensity and the sine of 3.6 times the gauze position had a linear relationship. This relationship is reasonable, as the  $R^2$  value is 0.9862, and the data points are scattered both sides of the line. However, on this graph there were often two data points for the same x value. This is because the sine function increased then decreased so in the first two graphs the same y value is reached twice. In an ideal world, these points would always be concurrent, and the distance between them represents the error in this experiment. The equation which this linear relationship represents is:

$$I = 78 \sin(3.6gp) + 8$$

Where I, is the sound intensity and gp is the gauze position. The gradient of the linear relationship was  $78 \pm 3$ , and this represents the amplitude of the sine function (of sound intensity vs. gauze position), or the maximum sound intensity achieved. The intercept is  $8 \pm 2$  dB, and this represents the background noise picked up by the microphone.

The linear relationship did not continue when the gauze was in the top half of the tube, as the sinusoidal function predicted negative sound intensities, which are impossible.

#### 9.6.5. Conclusions and Reflections

The hypothesis was supported; the position of the gauze in the lower half of the tube had a sinusoidal relationship with the sound intensity, the relationship is:  $I = 78 \sin(3.6gp) + 8$

It was felt that the errors and uncertainties in this experiment were quite large, and only just acceptable, the main reason for this was the unpredictable background noise, so the experiment could be improved by conducting the experiment in a silent environment, or one with a uniform background noise.

### 9.7. Heating Time

#### 9.7.1. Hypothesis

As seen in section 6, the heat absorbed by the gauze is lost through convection to the air, conduction to the tube, and in the kinetic energy of the sound wave, so the singing time will depend on how long the heat from the gauze is greater than these loses. This is demonstrated in the following equation: when

$$\frac{dT_{gauze}}{dt} \leq \frac{1}{m_g c_g} \left( m_{air} c_{air} \frac{dT_{air}}{dt} + \frac{1}{16} \rho A v \omega^2 s_m^2 + kA \frac{dT_{tube}}{dt} \right)$$

The tube stops singing. Therefore, the singing time depends on the temperature or heat absorbed by the gauze just before it starts singing. The temperature of the gauze while heating

can be modelled by: (Newton's law of Cooling)  $\frac{dT_{gauze}}{dt} = kA(T_{bunsen} - T_{gauze})$  This means

that initially, when the gauze is cold, it will heat very quickly so  $T_{bunsen} - T_{gauze}$  is large, but as the gauze heats up, there will be a smaller temperature difference, until heating the gauze any longer won't make much difference. When you differentiate Newton's law of cooling and heating, you get a logarithmic relationship between the heating time and the temperature of the gauze. We could not derive the exact relationship between singing time and temperature of the gauze (and therefore heating time), due to the large number of variables in the heat transfer equation above, however the logarithmic relationship will still be present.

### 9.7.3. Results

Heating time	Singing time
2	0
3	0
4	2
5	6
10	13
30	21
60	26
120	29

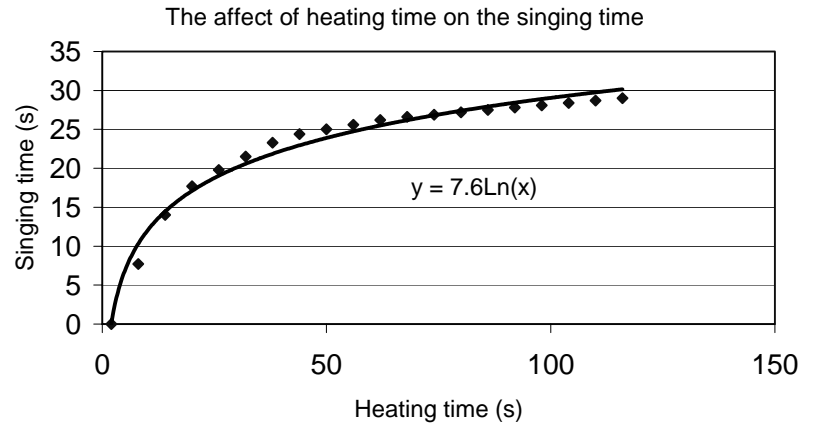


Figure 11 Graphed results from the Heating Time experiment

### 9.7.4. Discussion

Experimentally, there was a logarithmic relationship between heating and singing time. This relationship is reasonable, since the  $R^2$  value is 0.9872, and the uncertainties are small, but the scatter of points indicates that there may be other factors of consideration. This may be due to the effect of heating the air around the gauze at the same time as heating the gauze. This supports the hypothesis that the relationship between heating time and singing time should be logarithmic because singing time is approximately proportional to the temperature of the gauze (after heating), and the temperature of the gauze after heating has a logarithmic relationship with heating time.

### 9.7.5. Conclusions and Reflections

As predicted, increasing the heating time increased the singing time, in the relationship.  $t_{\text{singing}} = 7.6 \ln(t_{\text{heating}})$ . It was felt that this experiment could be improved if the gauze could be electrically heated, as then the amount of heat could be calculated directly from the amount of electrical energy put in. This would simplify equations and reduce error; however, unfortunately we did not have access to the voltages required. Further investigations into measuring the temperature inside the tube, around the gauze with a thermocouple array would help to determine if Newton's law can really be applied, in that it is justified to treat the system as a closed system with just the gauze and the Bunsen burner flame.

## 10. Summary

The singing tube phenomenon is caused primarily by a compression drawing in cool air, which encounters the gauze, heats and increases in pressure, this adds to the pressure maximum. The optimum gauze position is determined by where the most cool air will be drawn in, and where the cool air's pressure changes will have the most effect. The Rayleigh Criterion and the Rayleigh Index model this, causing the sound intensity,  $I$ , to have a sinusoidal relationship with gauze position ( $gp$ , measured in percent):  $I = 78 \sin(3.6gp) + 8$

The standing wave, which this sets up, has a frequency determined by the tube length and diameter. The frequency is also determined by the  $f = 175.5 \left( \frac{1}{L + 0.4d} \right)$  diameter through the expression:

The  $f^2 = -30000 \frac{k}{mc} + 50000$  thermal conductivity,  $k$ , of the tube material in the relationship:

standing wave is longitudinal, so is mainly unaffected by changes to the shape of the tube.

The heat transferred from the hot gauze to the air, tube and acoustic wave can be modelled by the expression:  $m_g c_g \frac{dT_{gauze}}{dt} = m_{air} c_{air} \frac{dT_{air}}{dt} + \frac{1}{16} \rho A v \omega^2 s_m^2 + kA \frac{dT_{tube}}{dt}$

This expression and Newton's law of Cooling lead to the relationship between the time the gauze is heated, and the time the tube sings:  $t_{sings} = 7.6 \ln(t_{heated})$ .

This applicable and interesting problem has been thoroughly investigated, and many relationships have been found. The discovery of the relationship between gauze position and sound intensity:  $I = 78 \sin(3.6gp) + 8$  is of particular scientific significance. This is because if the maximum sound intensity allowable by a system (such as the vibration limit at which a jet engine would start to break up) is known, then this equation can effectively predict where and where not a heat source must be located in order to prevent these dangerous vibrations. For example, the optimum point of fuel ignition in a jet engine can be determined.

### Acknowledgements

I would like to thank the whole Brisbane Girls Grammar School science department, for allowing me to interrupt their lessons with a rather loud 'singing' noise. Thanks also to Mr. Bromiley and Dr. Dancer who showed me how to manipulate differential equations. My IYPT teammates, helped with conducting most of the experiments, and I would like to thank my parents, for letting me do maths and physics all weekend. Most of all, I would like to thank my physics teacher Mr. Allinson for his guidance, support, encouragement, and answering of many long, frantic emails late at night. Thank you.

### References

- [1] Halliday D, Resnick R. Fundamentals of physics. 3<sup>rd</sup> ed. Canada: John Wiley & Sons, Inc; 1988.
- [2] Zitzewitz P, Neff R, Davids M. Physics – principles and problems. New York: Merrill; 1995.
- [3] Umurhan OM. Exploration of fundamental matters of acoustic instabilities in combustion chambers. [Online]. 1999 [cited 2006 Apr 26]; Available from: URL:<http://ctr.stanford.edu/ResBriefs99/umurhan.pdf>
- [4] Lehrman R, Swartz C. Foundations of physics. Artarmon NSW: Holt-Saunders Pty Ltd; 1976.
- [5] Matveev K. Thermal acoustic instabilities in the Rijke tube: experiments and modelling. [Online]. 2003 [cited 2006 Feb 21]; Available from: URL:[http://etd.caltech.edu/etd/available/etd-03042003-102221/unrestricted/matveev\\_thesis.pdf](http://etd.caltech.edu/etd/available/etd-03042003-102221/unrestricted/matveev_thesis.pdf)
- [6] Culick FCE. Combustion instabilities in liquid rocket engines: fundamentals and control. [Online]. 2002 [cited 2006 July 29]; Available from: URL:<http://www.its.caltech.edu/~culick/shortc/shortc-ONERA.html>
- [7] Sarpotdar SM, Ananthkrishnan N, Sharma SD. The Rijke tube – a thermo acoustic device. [Online]. 2003 [cited 2006 Mar 3]; Available from: URL:<http://www.iisc.ernet.in/academy/resonance/Jan2003/pdf/Jan2003p59-71.pdf>

## **8 Problem № 11: Singing tube**

### *8.1. Solution of Australia*

#### *8.1.1. Review of solution of Australia*

### **Review of the solution of the problem number 11 – Singing tube**

A tube open at both ends is mounted vertically. Use a flame to generate sound from the tube. Investigate the phenomenon.

The problem itself is very interesting from both theoretical and experimental point of view. It opens possibilities to perform number of experiments on the high-school level with a great probability of success. Theory of the problem can be found in many articles under the keywords of Singing tube or Rijke tube. However, these solutions are not complete and allow further investigation of dependencies.

#### **Solution from Australia**

Solution presented by Kathryn Zealand fully develops the quality of the assignment into a serious high-quality paper. The structure is appropriate; begins with basic definitions and interpretation of the problem, continues by theory explanation and culminates by extensive comparison of theoretical and experimental results. All relevant parameters as length and diameter of the tube, shape of the tube, material of the tube, position and intensity of the heat source were examined. As a kind of “bonus” also exotic configurations as reversing of the air flow by vacuum cleaner or using “cold source” rather than “heat source” in the upper half of the tube were used. I would like to cite one sentence from a discussion part of the paper, covering the tube material dependences: “Although the hypothesis was proved incorrect, more interesting discoveries were made as a result”. It reflects the honesty, with which the work was performed and which is so often missing during YPT presentations and discussions.

Only minor suggestions to improve the paper can be done. The layout could show better by using a smaller line-spacing; this would also reduce the length of the paper, 26 pages may be considered as too much. Also pictures and graphs should be placed strictly within the printable area of the page and formulas should be centered in extra lines. Usage of gauze instead of the flame itself could be discussed more thorough.

In summary, the presented solution goes far further than I would expect. It is complete, accurate and clearly written. In IYPT grading I would not doubt to show the highest grade 10.

Dr. Martin Plesch  
Institute of Physics  
Slovak Academy of Sciences  
Dubravska cesta 9  
Bratislava 845 11  
Slovakia

## 9. Problem №12: Rolling magnet

### 9.1. Solution of Australia

#### Problem №12: Rolling magnet

Alexandra Price, Gregory Terrace, Spring Hill 4000, QLD Australia, Brisbane Girls Grammar School, s106863@bggs.qld.edu.au

#### The Problem

*Investigate the motion of a magnet as it rolls down an inclined plane.*

#### Abstract:

An investigation into the motion of a magnet as it rolls down an incline seems somewhat monotonous when first examined. However, extensive experimentation and research into this problem yields some unanticipated results. The Earth's magnetic field plays a significant role in changing the path of the magnet as it rolls down a plane. This report contains four principal investigations. First, the influence of the Earth's magnetic field on the motion of a magnet was investigated and it was found that the magnet deviates to different extents, depending on the orientation of the magnet with respect to the magnetic field. Second, the effect of varying the angle of incline was then examined. Third, the effect of changing the material of the incline was investigated using wood and aluminium ramps. Finally, further experimentation into the effect of the Earth's magnetic field's influence on neodymium magnets (super magnets), although not quantitatively analysed, showed that the magnet's strength can affect the motion of the magnet to a greater extent than the Earth's magnetic field.

### 1. Interpretation

#### 1.1 Interpretation of Problem

The problem states “investigate the motion of a magnet as it rolls down an inclined plane”. The Oxford English Dictionary (1) defines a magnet as “a piece of iron or steel to which the characteristic properties of loadstone have been imparted, either permanently or temporarily, by contact with another magnet, by induction, or by means of an electric current.” Rolling is the “action (on the part of something) of turning over and over” (1). In the case of a cylinder, it rotates around the centre of mass. Motion is the “process of moving” or of “undergoing a change of place” (1).

#### 1.2 Assumptions

This investigation has three principal assumptions. First, it is assumed that the magnet is cylindrical and therefore exhibits a rolling motion when released at the top of an inclined plane. Second, it is assumed that the frictional forces exhibited on the magnet during its motion are sufficient to ensure the magnet only rolls down the plane and does not exhibit a sliding behaviour. Third, it is assumed that the environment the magnet is in has little interaction with the magnet (ie. no steel beams, air resistance).

## 2. Theory

### 2.1 Motion of a cylindrical object

#### 2.1.1 Dynamics Perspective

As the magnet rolls down the inclined plane, its magnetic field interacts with the Earth's magnetic field. The motion of the magnet down the slope is most easily analysed by breaking it into its constituent components (figure 1).

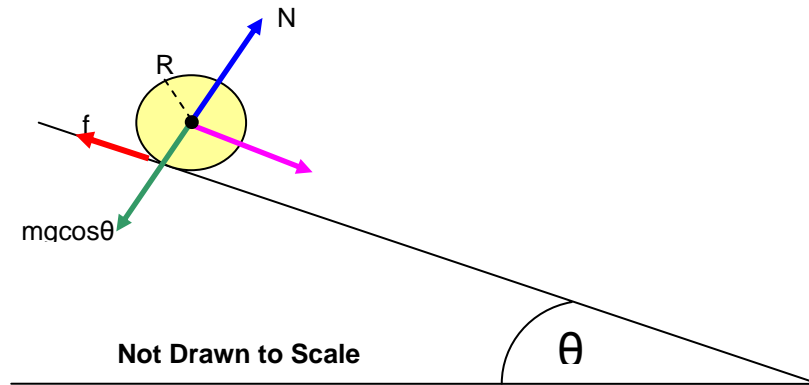


Figure 1 Components of a Rolling Cylinder

For a cylinder to roll, static friction is required. It is assumed that the static friction coefficient ( $\mu_s$ ) is always large enough to satisfy (2):

$$f \geq \mu_s mg \cos \theta$$

where  $m$  is the mass of the cylinder,  $g$  is acceleration due to gravity and  $\theta$  is the angle. Taking this into account, the minimum static frictional force needed for rolling can be calculated

$$F = \frac{1}{3} mg \sin \theta$$

So, for a cylinder of mass 0.069kg, and an angle of  $1.15^\circ$  to the horizontal, the force down the plane is calculated to be 0.0045N down the plane. The translational motion of the rolling magnet along the incline was calculated (2-4)

$$F = mg \sin \theta - f = ma$$

So, for the same cylinder on the same incline, the force along the incline is 0.0090N. The rotational motion of the centre of mass (torque) was analysed (3)

$$\tau = I_{cm} \alpha$$

where  $\alpha$  is the angular acceleration and  $\alpha = \frac{a}{R}$  (3) ( $a$  is acceleration and  $R$  is the radius of the cylinder)  $I_{cm}$  is the inertia at the centre of mass. For this example, the torque calculated was  $2.86 \times 10^{-5}$  N around the magnet. Torque,  $\tau$ , can be thought of as a force at a distance, acting to turn the magnet. The best way to calculate torque is to split it up into components (figure 2).

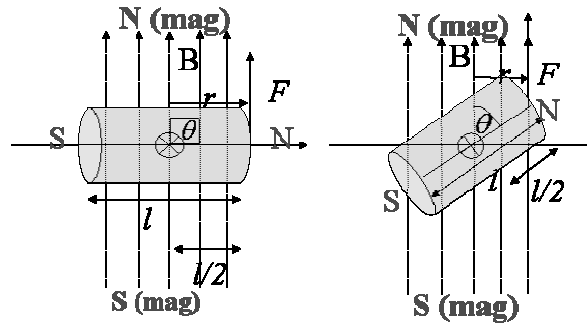


Figure 2 Components of torque for a rolling cylinder

To calculate the value of the torque, the following equation is used (4):  $\vec{\tau} = \vec{r} \times \vec{F}$  where  $\vec{F}$  is the force vector and  $\vec{r}$  is the vector from axis of rotation to point on which  $\vec{F}$  is acting.

In order to calculate the torque accurately, the restoring torque per unit of displacement was calculated. This enabled the effective work of the torque at any angle to be calculated and hence, the forces acting on the magnet. The period of oscillation was calculated

$$T = 2\pi \sqrt{\frac{I}{k}}$$

where  $I$  is the moment of inertia of the oscillating body and  $k$  is the restoring torque per unit displacement in radians. For a solid disk, such as a cylindrical magnet, the moment of inertia at the centre of mass is equal to (3)

$$I_{cm} = MR^2/2$$

Where  $M$  is the mass of the cylinder and  $R$  is the radius. The period of oscillation for the magnet used in the following experiments was measured by suspending it on a string and as a result, the moment of inertia for the oscillating cylindrical body. In this case,  $k$  was found to equal  $4.78 \times 10^{-4}$  Nm/radian.

### 2.1.2 Energy Perspective

The motion of a cylindrical object can also be analysed from an energy perspective where its initial gravitational potential energy (GPE) is converted into kinetic energy as it rolls down the incline (5)

$$mgh = \frac{3}{4}mv^2$$

Where the kinetic energy incorporates both linear and rotational kinetic energy (3)

$$\frac{1}{2}mv^2 + \frac{1}{2}I_{cm}\omega^2 = \frac{3}{4}mv^2$$

with  $\omega$  representing the angular momentum of the cylinder. The velocity of the centre of mass of a sliding cylinder is (3)

$$v_{com} = \sqrt{2gh}$$

However, for a rolling cylinder, the velocity at the centre of mass is less than that of a sliding cylinder due to the potential energy being converted into both linear and rotational kinetic energy. Therefore, the velocity of the centre of mass of a rolling cylinder is (3)

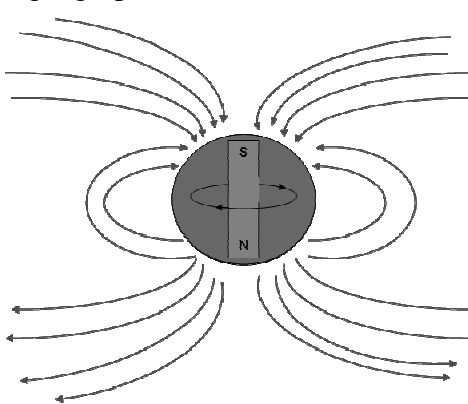
$$v_{com} = \sqrt{\frac{4}{3}gh}$$

For example, when the height of the ramp is 0.020m, the velocity at the centre of mass of a rolling cylinder is  $0.511\text{ms}^{-1}$ .

## 2.2 Effect of the Earth's magnetic field

### 2.2.1 The nature of the Earth's magnetic field

The Earth's north magnetic pole is located near the south geographic pole and the Earth's south magnetic pole is located near the north geographical pole (5). The angle between the Earth's north geographic pole and its North magnetic pole is called the angle of declination. Presently, this angle is approximately  $10^\circ$  (6). The Earth's south magnetic pole is actually the same as the south pole of a bar magnet and the Earth's north magnetic pole is actually a north pole of a bar magnet (figure 3). However, the magnetic axis is not aligned in the same position as its geographic axis. In fact, magnetic north is approximately 1000km away from geographic north (5). This is best visualised by figure 3 where the red arrows represent the



Earth's magnetic field lines and the black circular arrow in the centre represents the direction of the Earth's rotation.

The angle of the Earth's magnetic field in Brisbane is about  $56^\circ$  to the horizontal (ground) (6) (figure 4). However, it is very weak at the surface because the surface is along way from the Earth's dipole, having a total intensity of 0.05mT (6,7). The Earth's magnetic field extends over such a large area that the strength of the magnetic field is very uniform if you look at it over a large region (7).

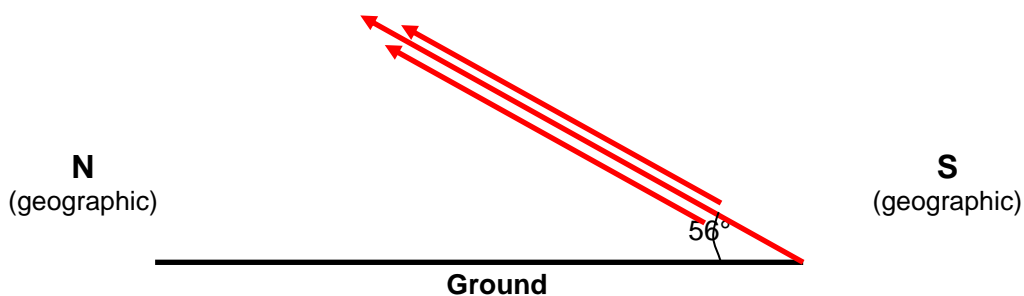
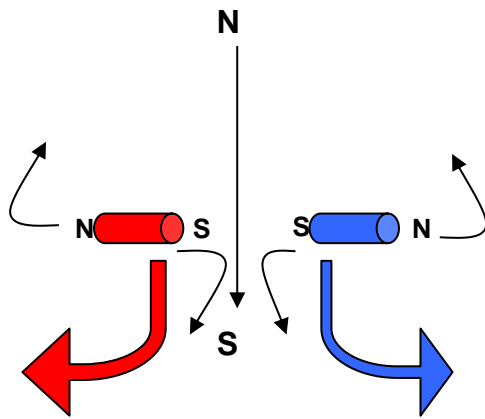


Figure 4 The Angle of the Earth's Magnetic field in Brisbane, Australia (5)

## 2.2.2 The effect of the Earth's magnetic field on a magnet

As a result of like poles repelling each other and unlike poles attracting each other (8), the Earth's magnetic field interacts with the rolling magnet without physical contact (9). As a magnet rolls down a plane from magnetic south to magnetic north (geographical north to south) it deviates because of interactions with the Earth's magnetic field depending on the orientation of the magnet.



**Figure 5 Effect of the Earth's magnetic field on a magnet**

As a magnet rolls down a plane, its north pole will attract to the Earth's magnetic South Pole, causing it to rotate. At the same time, the magnet's South Pole is attracted to the Earth's magnetic north pole. This concept is best envisaged by examining figure 5 where the ramp is positioned so that the magnet rolls down the incline from magnetic south to magnetic north. The best way to think of this interaction in order to investigate it quantitatively is to think of the magnet and the Earth's magnetic field as two separate magnets.

## 2.3 Aluminium

### 2.3.1 Eddy Currents

A cylindrical magnet has a magnetic field travelling from one pole to the other (figure 6). As the magnet rolls down the aluminium, its magnetic field cuts the aluminium sheet producing eddy currents which repel the magnet.

Eddy currents are caused by a moving magnetic field as it intersects a conductor (5). The relative motion causes a circulating flow of electrons or currents within the conductor.

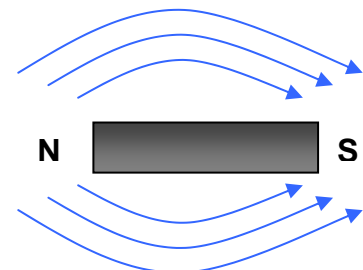


**Figure 6 Eddy Currents**

These circulating eddies of current create temporary electromagnets with magnetic fields that oppose the magnetic field of the magnet (figure 7).

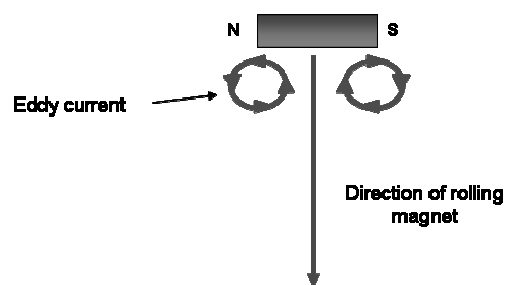


**Figure 7 Eddy Currents**

### 2.3.2 Lenz's Law

Lenz's law states that 'the current induced in a conductor by a changing magnetic field is in such a direction that its own induced magnetic field opposes the change that produced it' (5). In the case of the magnet, as it rolls down the aluminium plane, eddy currents are induced and the eddy current's own induced magnetic field opposes the change that produced it (ie. the magnet).

### 3. Experimental

3.1 How will varying the direction of the ramp affect the motion of the magnet?

#### 3.1.1 Observations

The magnet was observed to deviate less at the start of the roll and deviate more near the end of the plane.

#### 3.1.2 Results

The magnet's magnetic field strength was measured to be 36mT using a Pasco magnetic field sensor.

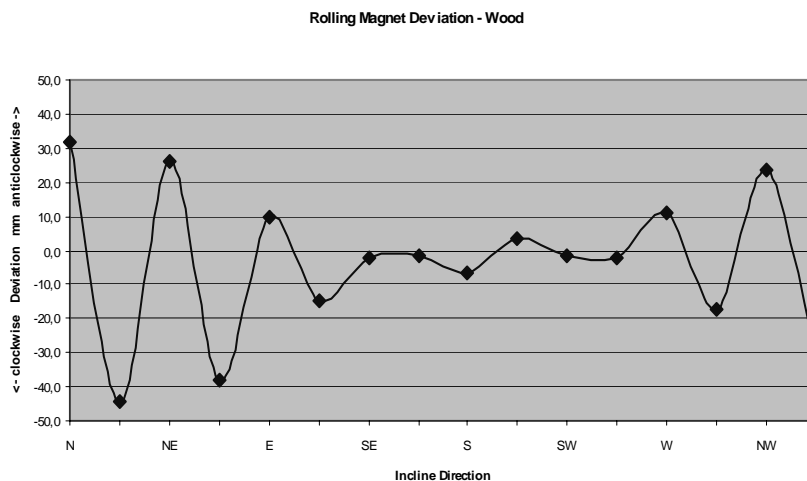
Deflection - Wood

Direction travelling	N		NE		E		SE		S		SW		W		W	
Mag N	E	W	SE	NW	S	N	SW	NE	W	E	NW	SE	N	S	NE	SW
Average	3.87	3.89	4.04	4.10	4.07	4.01	4.27	4.19	4.03	4.00	3.99	3.98	4.14	4.09	4.12	4.16
Spread	0.10	0.12	0.25	0.15	0.11	0.23	0.19	0.20	0.11	0.19	0.25	0.15	0.18	0.28	0.16	0.21
Deviation	0.06	0.07	0.17	0.08	0.07	0.14	0.12	0.12	0.06	0.11	0.18	0.08	0.09	0.20	0.11	0.11

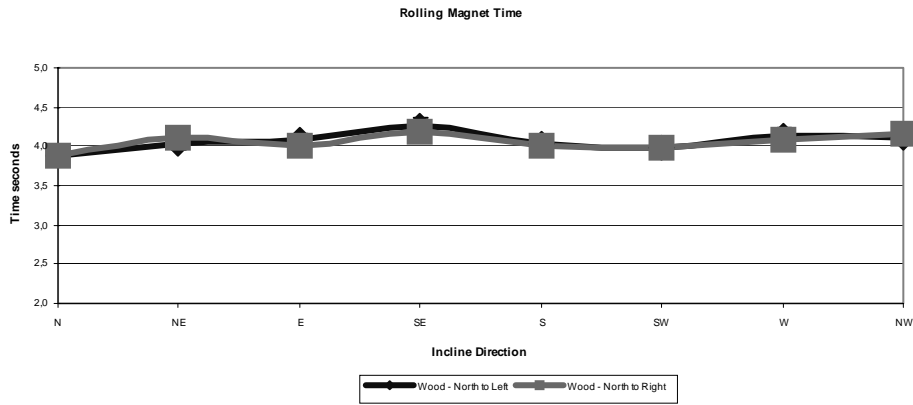
Where 'Mag N' represents the direction the north pole of the magnet points to.

**Table 2 Time Results**

#### 3.1.3 Analysis of Results



This graph represents the deviation of the magnet when it rolled down the wooden plane. The two x-values for each of the magnetic directions represent the magnet's north pole facing one direction and then flipped (ie. facing east, then facing west). The negative values indicate that the magnet travelled in a clockwise direction and the positive values indicate that the magnet travelled in an anticlockwise direction.



### 3.1.4 Discussion

The graph indicating the deviation of the magnet as it rolls down the wooden plane shows that changing the direction of the ramp results in a change in the deviation of the magnet i.e. the deviation of a magnet is dependant on the direction of the ramp, supporting the hypothesis. Although the Earth’s magnetic field only has a total intensity of 0.052mT in Brisbane, the angle of inclination of the Earth’s magnetic field (56° to the horizontal) could have an effect on the magnet’s motion as it rolls down the inclined plane. For example, as the magnet rolls down the ramp towards north, with its north pole facing east, the magnet deviates significantly in an anticlockwise direction. This is because the north pole of the magnet is ‘north-seeking’ and is therefore attracted to the Earth’s magnetic north pole. However, when the magnet’s north pole was facing east, and rolling in a southerly direction, the magnet only slightly deviated in an anticlockwise direction. The variation in deviation when comparing the deviation of the magnet rolling north and rolling south is attributed to the magnitude and direction of the resultant vectors produced from the Earth’s magnetic field and the angle of incline of the ramp. Where the red arrow represents the direction the magnet is traveling on the ramp, at an angle of 1.15°. The blue arrows represent the inclination of the Earth’s magnetic field and the dotted arrows represent the resultant vectors from each addition. This force is translated into torque and the magnet is rotated. When the magnet rolls in a southerly direction, the resultant force is nowhere near as large, as a result, little deviation occurs.

The increase in deviation as the magnet rolled down the plane (an observation) is attributed to it traveling at a faster speed near the end and the effect of torque. This means that friction plays less of a role in opposing the force that is turning the magnet. It also means that once the magnet has been forced slightly off its straight path, the deviation will continue to grow regardless of external magnetic forces. This deviation (excluding any external magnetic force) can be modeled by the equation  $F = mg \sin \theta \cos \alpha$  and used to estimate the final position of the magnet as it rolls down the plane. In a real situation, with the external magnetic force present during the whole experiment, the deviation would be greater than calculated using this formula.

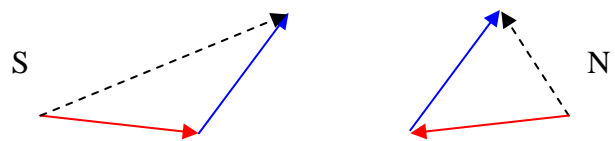
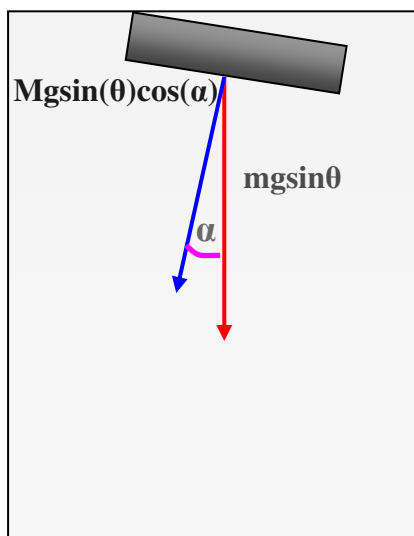


Figure 11. Resultant vectors



The graph of time versus direction shows, within experimental error, that the time taken for a magnet to roll down the plane with its north pole facing one direction is the same as when the magnet's north pole is facing  $180^\circ$  (the other direction). When the magnet was rolling north, it rolled down the ramp in the smallest time. This is probably due to the fact that the magnet is rolling down 'with' the Earth's magnetic field. This would have a resultant force with a large vector down the plane, meaning that the magnet would receive an extra 'push' of energy that it would not receive if it was traveling any other direction. The peak in time when traveling southeast is attributed to the magnet deviating the magnet in a clockwise direction for both trials.

The magnet making a moderately loud sound as it rolled down the ramp is attributed to the 15% friction between the two surfaces which was converted into heat and sound energy. Every effort was made to ensure the trials were as analogous as possible. Each time the ramp was reorientated, the magnet was placed at least twenty metres away to ensure minimal interaction. Experiments were also conducted in a wooden house on a wooden table and as far away from any steel beam supports as possible. However, it is highly likely, due to possible compass errors, that the ramp could have been misaligned by several degrees, therefore altering the results. During experimentation, the ramp was wiped down with a slightly damp cloth and left to dry every so often to try and prevent excess friction due to dust and moisture particles. In order to minimize error in timing, the person with the stop watch was the one who released the magnet. Much thought was put into deciding the most accurate process to measure the deviation of the magnet.

### 3.1.9 Conclusions

As the magnet rolls down the ramp, it tries to align its poles with the Earth's magnetic poles and as a result, the magnet deviates as it rolls. The deviation of the magnet from the weight force providing the magnet has been misaligned (due to an external magnetic force) can be modeled by the equation  $F = mg \sin \theta \cos \alpha$  and used to estimate the final position of the magnet as it rolls down the plane.

## 3.2 How will varying the angle of incline affect the motion of the magnet?

### 3.2.1 Hypothesis

As the angle of incline is increased, the deviation will increase until a critical angle is reached.

### 3.2.2 Observations

By raising the angle of the incline, the magnet was observed to have deviated more. However, if the ramp was raised past a critical angle (around 25 degrees), the magnet exhibited a sliding behavior instead of rolling behavior.

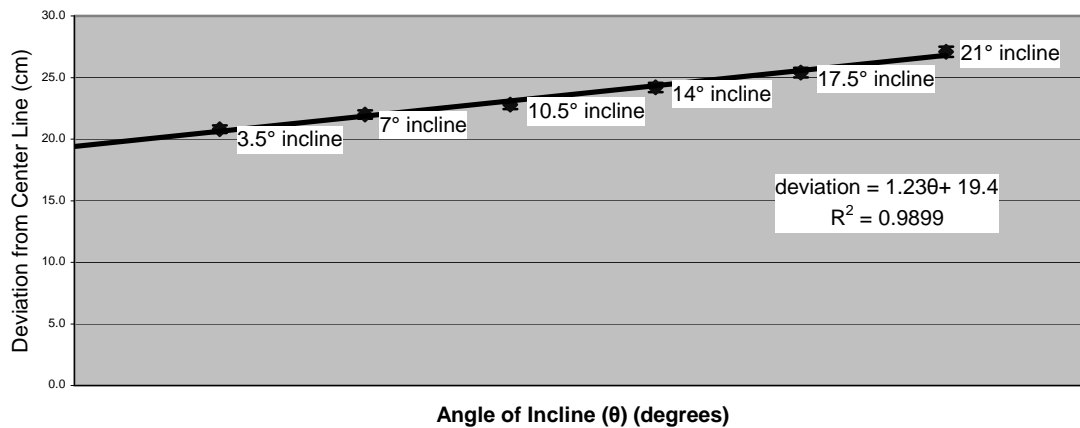
### 3.2.3 Results

**Table 3 Deviation Results**

	3.5° incline	7° incline	10.5° incline	14° incline	17.5° incline	21° incline
Average	20.8	22.0	22.8	24.2	25.4	27.1
Spread	0.8	0.9	0.5	0.7	0.9	0.5
Deviation	0.5	0.5	0.3	0.4	0.5	0.3

### 3.2.4 Analysis of Results

Deviation from Centre Line Vs Angle of Incline



### 3.2.5 Discussion

The graph and its y-intercept value of  $19.4 \pm 0.3$ , indicate that, within experimental error, the deviation of a magnet from the centre line is directly proportional to the angle of the incline the ramp is placed at, provided the material and all other physical conditions remain constant. The slope of the graph of deviation from centre line versus angle of incline within the calculated experimental error of 0.02 equals 1.23 meaning that the deviation of the incline increases at the rate of  $1.23\text{cm}/^\circ$ . So, for every degree the incline is increased by, the deviation of the magnet from the centre line is increased by 1.23cm. The straight trendline and its  $R^2$  value of 0.9899 indicates that the ratio of deviation to angle of incline is constant up to and including an angle of incline of  $21^\circ$ . The results therefore support the hypothesis saying that as the angle of incline is increased, the deviation will increase. However, using the graph, the relationship between the deviation and the angle of incline once the angle of incline is above  $21^\circ$  was not able to be modelled.

The sliding behavior exhibited by the magnet occurred because the resolved component of the weight force down the plane provides a greater acceleration negating the frictional force that turns it ie.  $f > \mu_s mg \cos \theta$ . Given that the sliding behavior was observed when the angle of inclination was greater than  $25^\circ$ , an approximation for the coefficient of static friction can be calculated. To do this, we assume that the force down the plane (F) is equal to the force of friction (f) and for the purpose of the following calculation, it is assumed that  $25^\circ$  is the angle at which the rolling cylinder began to slide.

$$F = f \leftrightarrow ma = \mu_s mg \cos \theta$$

$$a = \mu_s \times g \times \cos \theta \leftrightarrow g \sin \theta = \mu_s \times g \times \cos \theta$$

$$\sin \theta = \mu_s \times \cos \theta \leftrightarrow \mu_s = \frac{\sin \theta}{\cos \theta} = \tan \theta$$

$$\therefore \mu_s \approx \tan 25^\circ \approx 0.467$$

Given the inaccuracy of this calculation, due to having to guess the critical angle, this calculation of the coefficient of static friction,  $\mu_s$ , is further substantiated by Kurtus which states that the coefficient of static friction for metal on glass is 0.5-0.7 (9). If the magnet began to exhibit a sliding behaviour, the magnet would travel faster down the plane than a rolling magnet because all of a sliding magnet's potential energy is converted into linear kinetic energy whereas a rolling magnet's potential energy is converted into both linear and rotational kinetic energy.

Due to the fact that a camera was unable to be used in recording the deviation, there is more likely to be error associated with the measurement of the deviation. While every effort was taken to eliminate error, the experimentation was conducted inside a concrete physics laboratory building which increases the likelihood of errors in the measurements due to an interaction with other magnetic materials, such as a steel support beam. I was also unable to find a level, so the longitudinal level was unable to be verified. There were also some significant vibrations occurring in the classroom due to other people conducting experiments with low frequencies. These vibrations may have caused error in the deviations.

### 3.2.6 Conclusions

The results support the hypothesis in saying that within experimental error, a plot of deviation of magnet from the centreline versus angle of incline results in a linear relationship up until and including  $21^\circ$ .

## 3.3 How will varying the material of the incline affect the motion of the magnet?

### 3.3.1 Hypothesis

Using an aluminium incline, as opposed to a wood incline, although having less friction, will result in a slower time and a larger deviation of the magnet, due to eddy currents being created as the magnet moves and acting to oppose the motion of the magnet.

### 3.3.2 Observations

For the majority of trials, the magnet was observed to deviate more on the aluminium plane than on the wooden plane. The time taken for the magnet to roll down the aluminium plane was significantly greater than the time taken to roll down a wooden plane.

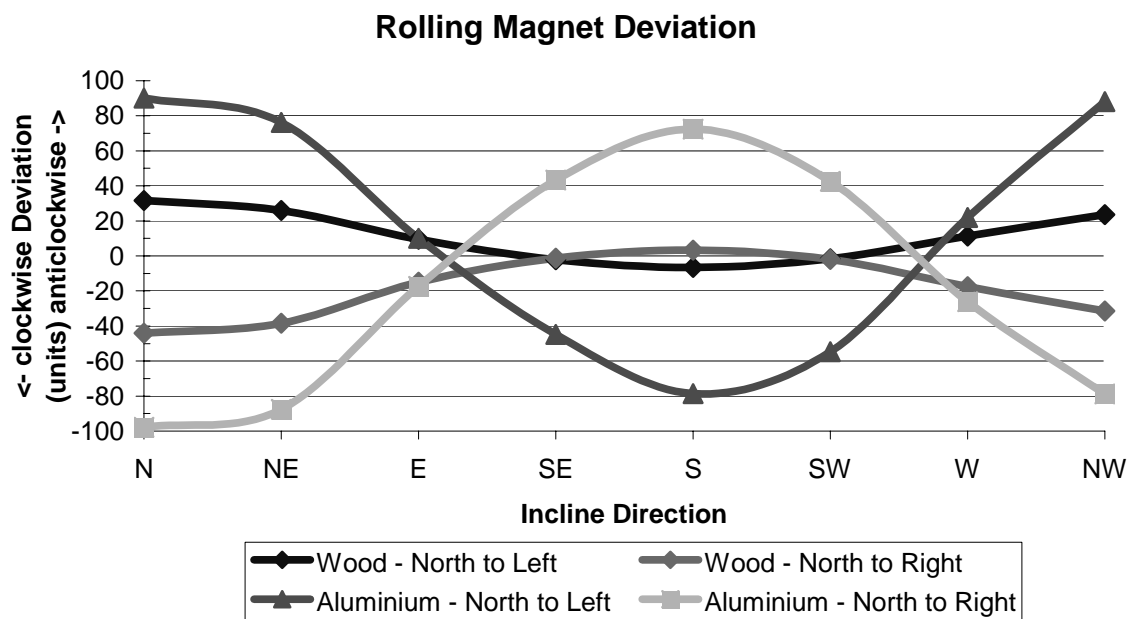
## Results

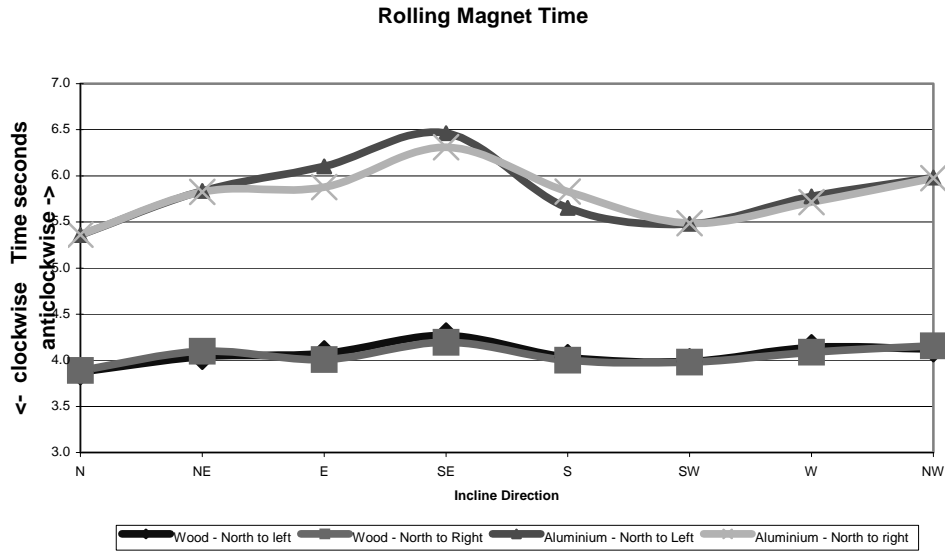
Deflection - Aluminium																
	N		NE		E		SE		S		SW		W		NW	
Mag N	E	W	SE	NW	S	N	SW	NE	W	E	NW	SE	N	S	NE	SW
Average	90.1	-97.8	76.2	-87.5	10.0	-17.3	-44.8	43.4	-78.7	72.4	-54.6	42.6	21.9	-26.1	88.1	-78.8
Spread	4.0	3.0	3.0	5.0	3.0	2.0	4.0	7.0	5.0	5.0	5.0	5.0	2.0	4.0	5.0	6.0
Deviation	2.1	1.8	1.8	3.5	2.0	1.3	1.8	3.6	2.7	2.6	2.6	2.6	1.1	2.1	2.9	3.8

**Table 4. Deviation on Aluminium Results**

	N		NE		E		SE		S		SW		W		NW	
Mag N	E	W	SE	NW	S	N	SW	NE	W	E	NW	SE	N	S	NE	SW
Average	5.36	5.36	5.84	5.83	6.10	5.88	6.46	6.31	5.65	5.83	5.48	5.49	5.78	5.71	5.98	5.98
Spread	0.12	0.09	0.18	0.24	0.13	0.14	0.19	0.14	0.32	0.33	0.20	0.30	0.33	0.26	0.23	0.24
Deviation	0.07	0.06	0.07	0.15	0.08	0.07	0.13	0.08	0.19	0.18	0.12	0.15	0.17	0.19	0.12	0.14

**Table 5. Time on Aluminium Results**  
Analysis of Results

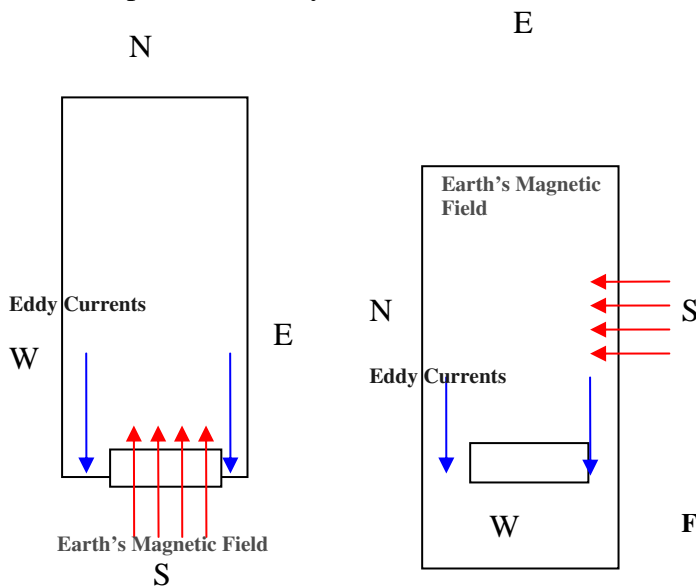




### 3.3.3 Discussion

The graph showing deviation of the magnet on material versus incline direction shows that the deviation of the magnet, when rolled down an aluminium ramp is much greater than on wood. All lines follow similar curved relationships as the incline direction changes.

The deviation of the magnet on both aluminium and wood is the same when the ramp rolled east. The minimum deviation for the magnet on aluminium occurs when it is travelling east and west (approximately). This is because as the magnet rolls down the plane towards the east (for example), the eddy



currents produced are in a direction perpendicular to the earth's magnetic field. As a result, there is no parallel force vector which adds to changing the direction of motion.

When the magnet is rolling due north on aluminium, the eddy currents have to act against the Earth's magnetic field

Figure 13. Rolling North on Aluminium

Figure 12. Rolling East on Aluminium

The time taken for the magnet to roll down the aluminium plane was significantly greater than the time taken to roll down a wooden plane which is attributed to eddy currents opposing the magnet's motion as it rolled down the plane.

In order to attempt to calculate the effects of the eddy currents produced in the aluminium, it was assumed that both the aluminium and wood had a similar static coefficient of friction,  $\mu_s$ . In actual fact, the wood had a slightly larger  $\mu_s$ . This was measured by rolling down a

non-magnetic cylinder of similar size to the magnet down each plane and measuring the time taken for it to reach the end of the ramp.

<p><u>Calculation of Current:</u>  <math>P = I^2R = J/s = 0.008J/5.81s = 0.00138J/s</math></p> <p><math>I^2R = 0.00138J/s</math>  <math>I = (0.00138/2.65 \times 10^{-5})^{0.5} = 7.2 \text{ amps}</math></p> <p><math>EMF = IR = 7.2 \times 2.65 \times 10^{-5} = 1.9 \times 10^{-4}V</math></p> <p><u>Calculation of temperature increase:</u>  <math>Shc = \text{Energy} \times \text{mass}^{-1} \times \text{Temperature}^{-1} = J \times \text{kg}^{-1} \times K^{-1}</math></p> <p>Therefore,  <math>T = \text{Energy} \times \text{mass}^{-1} \times \text{specific heat}^{-1} = J \times \text{kg}^{-1} \times (J \times \text{kg}^{-1} \times K^{-1})^{-1} = K</math></p> <p><math>T = 0.008J/3.24\text{kg}/900 = 2.74 \times 10^{-6}K</math></p> <p>There is no temperature increase which could be observed.</p>	<p>Energy lost by magnet:            On wood (<math>E_w</math>) = 0.002J            On aluminium (<math>E_{al}</math>) = 0.010J  <math>E_{al} - E_w = 0.008J</math></p> <p>Area of eddies = <math>0.0025m^2</math>            Av vel wood (<math>v_w</math>) = <math>0.48ms^{-1}</math>            Av vel aluminium (<math>v_{al}</math>) = <math>0.33ms^{-1}</math></p> <p>Resistance of Al = <math>2.65 \times 10^{-5} \Omega</math>            Weight of whole Al = 3.24kg            Vol of Al = <math>0.0012m^3</math></p>
---	---

With a temperature increase of  $2.74 \times 10^{-6}K$ , even with the large number of trials completed, the temperature increase would be negligible because any increase would be lost to the surrounding environment. Using the previous calculation for current and as a result EMF, it is possible to measure the magnetic field created to oppose the motion of the magnet as it rolled down the aluminium plane.

Where  $F_E$  is the force of the electric field,  $F_B$  is the force of the magnetic field,  $q$  is the charge on an electron,  $E$  is the electric field strength,  $v$  is velocity,  $B$  is the magnetic field strength,  $V$  is the voltage,  $d$  is distance,  $EMF$  is the induced voltage and  $L$  is the length of the conductor. For the purpose of this calculation, the length of the conductor was taken to be the diameter of the eddy currents combined. Given that the magnetic field strength of the magnet was found to be 36mT, the value for the eddy current's magnetic field strength of 7.35mT is acceptable.

$$F_E = F_B \rightarrow qE = qvB$$

$$E = vB \rightarrow \frac{V}{d} = \frac{EMF}{L} = vB$$

$$\frac{1.9 \times 10^{-4}}{0.08} = 0.33B$$

$$B = 7.35mT$$

$v = 0.33ms^{-1}$ $EMF = 1.9 \times 10^{-4}V$ $L = 0.08m$
---

The deviation of the magnet on aluminium when travelling south was 75% of the deviation value when the magnet was rolling north. However, the deviation of the magnet when rolling south on wood was a mere 25% of the deviation recorded when the magnet rolled north. This is most likely attributed to the eddy currents creating a significantly stronger force than the Earth's magnetic field, meaning that it has more influence over the motion of the magnet than

the Earth's magnetic field does. On both the wood and aluminium ramps, the time taken for the magnet to roll down the plane was greatest when it rolled in a south east direction and shortest when it rolled north. Although it is very difficult to produce a justifiable explanation as to why this occurred, the most likely cause is due to the angle of inclination of the Earth's magnetic field.

Errors for this experiment could have occurred due to the aluminium becoming dirty and irregular. The error associated with this was minimised by wiping down the aluminium regularly with a damp cloth and leaving it to dry. The deviation scale was sticky taped onto the aluminium surface, so this could have interrupted the most of the magnet just before it crossed the deviation scale. This error was minimised by ensuring a single piece of sticky tape ran across the front edge of the scale and was pressed flat against the aluminium. A hand was placed on the ramp after each trial to ensure any residual currents in the aluminium were removed. The same precautions and error minimising steps were taken in this experiment as in experiment one.

### 3.3.4 Conclusion

The results support the hypothesis in saying that a magnet deviates to a greater extent on an aluminium plane than a wooden plane due to eddy currents created in the aluminium. These eddy currents oppose the motion of the magnet, causing it to roll down the ramp at a slower speed than on a wooden incline.

### 3.4 Investigation into motion near the edge (qualitative)

If the plane is aligned with the North-South field lines, the magnet still exhibits turning behaviour due to the eddy currents present in the aluminium. However, as the magnet approaches the edge of the aluminium, there are only eddy currents on one side of the magnet. This results in the magnet travelling back into the middle of the aluminium.

## 4 Conclusions

### 4.1 Conclusions for nonconductive planes

The magnet deviation depends on which way the poles are orientated due to interaction with the Earth's magnetic field. The larger the angle of the plane, the higher the deviation of the magnet.

### 4.2 Conclusions for conductive planes

When a magnet rolls down an aluminium plane, eddy currents are created in the aluminium which oppose the magnet's motion down the plane. When super magnets roll down an aluminium plane, the eddy currents are stronger which produces a stronger correcting force.

## 5 Acknowledgements

I would like to acknowledge the great deal of support and assistance I have received from Mr Allinson, his help and knowledge has been invaluable throughout my investigation.

## 6 Reference List

- [1] Oxford English Dictionary [book on CD-ROM]. 3rd ed. New York (NY): Oxford University Press; 2002.
- [2] Brito L, Fiolhais M, Paixao J. Cylinder on an incline as a fold catastrophe system. *Eur J Phys* 2003;24:115-23.
- [3] Resnick R, Halliday, D. *Physics Part 1*. 3rd Ed. New York: John Wiley & Sons; 1977.
- [4] Serway RA, Jewett JW. *Physics for Scientists and Engineers*. 6th ed. Belmont (CA): Thomson Learning; 2004.
- [5] Walding R, Rapkins G, Rossiter G. *New Century Senior Physics*. South Melbourne, Australia: Oxford University Press; 1999.
- [6] National Geophysical Data Centre (NGDC). Estimated Values of Magnetic Field Properties [Online]. 2004. [Cited 2006 May 18]; Available from: URL:<http://www.ngdc.noaa.gov/seg/geomag/jsp/IGRFGrid.jsp>
- [7] Tom. Magnet's floating in the Earth's field [Online]. [2001?] [cited 2006 Apr 13]; Available from: URL:[http://van.hep.uiuc.edu/van/qa/section/stuff\\_about\\_space/the\\_earth\\_and\\_the\\_moon.html](http://van.hep.uiuc.edu/van/qa/section/stuff_about_space/the_earth_and_the_moon.html)
- [8] Magnetic fields and how to make them [Online]. 1999 [cited 2006 Apr 13]; Available from: URL:<http://physics.bu.edu/~duffy/PY106/MagField.html>
- [9] Ron K. Lab Mag Field Lines [Online]. 2001? [Cited 2006 Apr 13]; Available from: URL:[http://www.emporia.edu/physics/keithron/collegelab2/magnetic\\_lines.htm](http://www.emporia.edu/physics/keithron/collegelab2/magnetic_lines.htm)